



Titre: Title:	A homotopy analysis method for forced transverse vibrations of simply supported double-beam systems with a nonlinear inner layer
Auteurs: Authors:	Kabutakapua Kakanda, Hongbo Zhu, Herman Musumari Siaben, Panick Kalambay, Zhaolong Han, Yan Bao, Mengmeng Zhang, & Dai Zhou
Date:	2023
Type:	Article de revue / Article
Référence: Citation:	Kakanda, K., Zhu, H., Siaben, H. M., Kalambay, P., Han, Z., Bao, Y., Zhang, M., & Zhou, D. (2023). A homotopy analysis method for forced transverse vibrations of simply supported double-beam systems with a nonlinear inner layer. AIP Advances, 13(7), 24 pages. https://doi.org/10.1063/5.0156487

 **Document en libre accès dans PolyPublie**
Open Access document in PolyPublie








URL de PolyPublie: PolyPublie URL:	https://publications.polymtl.ca/54805/
Version:	Révisé par les pairs / Refereed
Conditions d'utilisation: Terms of Use:	CC BY

 **Document publié chez l'éditeur officiel**
Document issued by the official publisher

Titre de la revue: Journal Title:	AIP Advances (vol. 13, no. 7)
Maison d'édition: Publisher:	AIP Publishing
URL officiel: Official URL:	https://doi.org/10.1063/5.0156487
Mention légale: Legal notice:	© 2023 Author(s). All article content, except where otherwise noted, is licensed under a Creative Commons Attribution (CC BY) license (http://creativecommons.org/licenses/by/4.0/). https://doi.org/10.1063/5.0156487

RESEARCH ARTICLE | JULY 05 2023

A homotopy analysis method for forced transverse vibrations of simply supported double-beam systems with a nonlinear inner layer

Kabutakapua Kakanda ; Hongbo Zhu ; Musumari Herman; Panick Kalambay; Zhaolong Han  ; Yan Bao ; Mengmeng Zhang ; Dai Zhou 



AIP Advances 13, 075103 (2023)

<https://doi.org/10.1063/5.0156487>



View
Online



Export
Citation

CrossMark

Articles You May Be Interested In

Analytic approximate solutions to electrically actuated MEMS

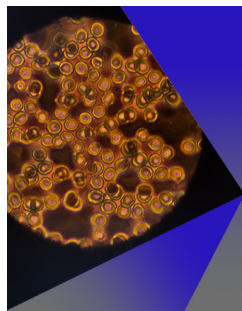
AIP Conference Proceedings (November 2020)

Partitioning lower bounds for Bubnov–Galerkin's eigenvalues

J. Math. Phys. (December 1981)

Mathematical modeling of three-layer circular plate under uniformly distributed load (pressure)

AIP Conference Proceedings (March 2015)



AIP Advances

Special Topic: Medical Applications
of Nanoscience and Nanotechnology

Submit Today!

 AIP
Publishing

A homotopy analysis method for forced transverse vibrations of simply supported double-beam systems with a nonlinear inner layer

Cite as: AIP Advances 13, 075103 (2023); doi: 10.1063/5.0156487

Submitted: 30 April 2023 • Accepted: 8 June 2023 •

Published Online: 5 July 2023



View Online



Export Citation



CrossMark

Kabutakapua Kakanda,¹  Hongbo Zhu,¹  Musumari Herman,² Panick Kalambay,³ Zhaolong Han,^{1,a)} 
Yan Bao,¹  Mengmeng Zhang,¹  and Dai Zhou¹ 

AFFILIATIONS

¹State Key Laboratory of Ocean Engineering and School of Naval Architecture, Ocean and Civil Engineering, Shanghai Jiao Tong University, Shanghai 200240, China

²Department of Civil, Geological, and Mining Engineering, Polytechnique Montreal, Montreal, Quebec H3T 1J4, Canada

³Department of Civil and Environmental Engineering, The University of North Carolina at Charlotte, Charlotte, North Carolina 28223, USA

^{a)}Author to whom correspondence should be addressed: han.arkey@sjtu.edu.cn

ABSTRACT

The present study introduces a novel algorithm based on the homotopy analysis method (HAM) to efficiently solve the equation of motion of simply supported transversely and axially loaded double-beam systems. The original HAM was developed for single partial differential equations (PDEs); the current formulation applies to systems of PDEs. The system of PDEs is derived by modeling two prismatic beams interconnected by a nonlinear inner layer as Euler–Bernoulli beams. We employ the Bubnov–Galerkin technique to turn the PDEs' system into a system of ordinary differential equations that is further solved with the HAM. The flexibility and straightforwardness of the HAM in computing time-dependent components of the system's transverse deflection and natural frequencies, in conjunction with the observed fast convergence, offer a robust semi-analytical method for analyzing such systems. Finally, the transverse deflection is built through the modal superposition principle. Thanks to a judicious and high-flexibility selection of initial guesses and convergence control parameters, numerical examples confirm that at most six iterations are needed to achieve convergence, and the results are consistent with the selected benchmark cases.

© 2023 Author(s). All article content, except where otherwise noted, is licensed under a Creative Commons Attribution (CC BY) license (<http://creativecommons.org/licenses/by/4.0/>). <https://doi.org/10.1063/5.0156487>

I. INTRODUCTION

Due to their role in many mechanical, civil, and aerospace engineering fields, double-beam systems have garnered tremendous interest in the scientific community. These systems are employed in modeling the behavior of various engineering structures, such as suspension and arc bridges, sandwich beams for aircraft components, and systems of interconnected pipelines, to achieve optimal design owing to their stiffness-to-weight and strength-to-weight ratios.

Double-beam systems are made of two parallel beams continuously connected by an inner layer. Due to the synergy between the two beams, the system is an excellent technique for mitigating structural vibrations.

While beams are typically modeled as Timoshenko,^{1–4} Euler–Bernoulli,^{5–8} and Rayleigh^{9,10} beams, the inner layer is typically modeled as Winkler,^{11–13} Pasternak,^{12–14} or Kerr¹⁰ layers.

Many methods based on reliable mathematical formulations for modeling double-beam systems are found in the literature. The pioneering work of Seeling and Hoppmann¹⁵ proposed a generic solution of n-bar systems described as Euler–Bernoulli beams for a two-bar system. Hamada *et al.*¹⁶ studied free and forced vibrations of double-beam systems using the extended finite integral transformation approach and Laplace transform. Another set of investigations contains the study conducted by Oniszczuk,¹⁷ where the classical modal expansion method was employed to analyze the forced transverse response of a double-beam system subjected to

arbitrarily distributed continuous loads. Before his study related to forced vibrations, Oniszczuk used a Bernoulli–Fourier method to solve free transverse vibration problems.¹⁸ Zhang *et al.*¹⁹ examined the effect of compressive axial loads on transverse vibrations through the modal expansion approach. Palmeri and Adhikari²⁰ considered a viscoelastic behavior of the inner layer and applied a Galerkin-type state-space approach to explore the transverse vibrations of slender double-beam systems. Han *et al.*¹¹ introduced a dynamic stiffness-based modal analysis to analyze the influence of the elastic inner layer composed of several elastic supports. Liu and Yang⁵ used a closed-form analytical approach called the distributed transfer function method to study the double-beam system with general boundary conditions. Brito *et al.*¹⁴ conducted the bending analysis of a double-beam system as Euler–Bernoulli beams with an elastic inner layer using a direct boundary element approach. Using Green’s functions, Zhao *et al.*³ analyzed the forced vibration of a Timoshenko double-beam system subjected to compressive axial loads.

As evidenced by the studies mentioned above, the analysis of double-beam systems has reached a mature stage. Nevertheless, some challenges remain and garner interest in developing new models. One of the challenges is related to the inner layer, which is often assumed to have linear behavior. Such a simplifying assumption is widely adopted to avoid cumbersome mathematical formulations in the case of analytical or semi-analytical methods. The same assumption is adopted to avoid computer-intensive numerical models, particularly when forced vibrations are investigated. Thus, for a thorough analysis, new methods must address the nonlinear behavior of the inner layer. In the literature, some studies that have addressed the nonlinear behavior of the inner layer or the foundation of a double-beam system^{21,22} or, generally, the nonlinear vibration of the system²³ are available; however, the influence of the nonlinear stiffness coefficient remains to be elucidated.

This paper aims to develop a novel HAM-based algorithm to address transverse vibrations of an axially and transversally loaded double-beam system composed of two prismatic beams modeled as Euler–Bernoulli beams continuously interconnected by a nonlinear inner layer.

The HAM was developed by Liao²⁴ and thoroughly explained in Ref. 25 by the same author. In the years following the seminal work of Liao, the HAM has proven to be an effective technique for solving complex and highly nonlinear equations of mechanical systems. This statement is confirmed by the tremendous amount of HAM-related work in the literature. As an analytical method, the HAM is easy to implement and less computer-intensive because it does not require system discretization. Moreover, the HAM relies on a flexible way of guaranteeing convergence; therefore, it provides a reasonably straightforward procedure for analytically approximating the solutions of nonlinear equations of mechanical systems.

Indeed, convergence is guaranteed and accelerated by an easy selection of the nonzero convergence-control parameter, the auxiliary function, and the initial guess of the solution. More importantly, unlike many other analytical and semi-analytical approaches for nonlinear systems, the HAM is independent of large or small parameters.

The HAM has been the foundation of several applications.^{26–30} Regarding beam analysis, the existing HAM-based models are limited to single beam problems. In Ref. 31, a robust formulation of the HAM was developed to address the transversal vibration of quintic nonlinear beams. In Ref. 32, the effectiveness and accuracy of the HAM were demonstrated through the investigation of large deformations of a single beam subjected to static, arbitrarily distributed loads. Another valuable HAM-based analytical approximation was proposed in Ref. 33, where large deformations of a cantilever beam made of axially and functionally graded material were investigated. In addition, for floating bridges with floating piers, the method established here may also be applied to analyze the coupled hydrodynamic-structural behavior by integrating this method with the multi-body hydrodynamic model established by Chen *et al.*³⁴ and Zou *et al.*³⁵ The method could also be used for analysis of ice–structure interaction by taking an ice sheet locally as a beam.³⁶ In the present study, the HAM is combined with the Bubnov–Galerkin technique to transform the system of PDEs describing the motion of a double system into a system of ODEs; the dynamic response is obtained through the modal superposition principle.

Besides the introduction, this paper is organized as follows: Sec. II presents the mathematical formulation of a double-beam model. In Sec. III, the HAM is applied to the system of ODEs derived in the previous section. Some numerical examples are solved in Sec. IV, and the concluding remarks are given in Sec. V.

II. MATHEMATICAL FORMULATION OF THE PROBLEM

The to-be-studied double-beam system is depicted in Fig. 1. The model comprises two parallel prismatic beams that are elastically and continuously connected by an inner layer modeled as a Winkler foundation, generally characterized by a mass per unit length denoted by μ and linear and nonlinear stiffness coefficients denoted by k_L and k_{NL} , respectively. The homogeneous and slender beams of identical length are characterized by flexural stiffness $E_i I_i$, densities ρ_i , and cross-sectional areas A_i ; they are axially loaded with compressive loads denoted by P_i and transversally loaded with dynamic point loads or continuously varying distributed forces denoted by f_i ($i = 1, 2$). The system of equations that governs the forced transverse vibrations of the beam system is derived from the Euler–Bernoulli theory and is given by the following equation:

$$\begin{cases} \frac{\partial^2}{\partial x^2} \left(E_1 I_1 \frac{\partial^2 w_1}{\partial x^2} \right) + P_1 \frac{\partial^2 w_1}{\partial x^2} + \frac{\mu}{4} \left(\frac{\partial^2 w_1}{\partial t^2} + \frac{\partial^2 w_2}{\partial t^2} \right) + \rho_1 A_1 \frac{\partial^2 w_1}{\partial t^2} + k_L (w_1 - w_2) \\ \quad + k_{NL} (w_1 - w_2)^3 = f_1, \\ \frac{\partial^2}{\partial x^2} \left(E_2 I_2 \frac{\partial^2 w_2}{\partial x^2} \right) + P_2 \frac{\partial^2 w_2}{\partial x^2} + \frac{\mu}{4} \left(\frac{\partial^2 w_1}{\partial t^2} + \frac{\partial^2 w_2}{\partial t^2} \right) + \rho_2 A_2 \frac{\partial^2 w_2}{\partial t^2} - k_L (w_1 - w_2) \\ \quad - k_{NL} (w_1 - w_2)^3 = f_2, \end{cases} \quad (1)$$

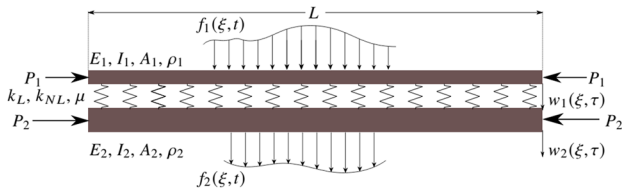


FIG. 1. Transversally and axially loaded double-beam system comprising an inner layer characterized by linear (k_L) and nonlinear (k_{NL}) stiffness coefficients and a mass per unit length μ .

with the initial conditions given as

$$w_i(x, 0) = w_{i0}(x), \dot{w}_i(x, 0) = \dot{w}_{i0}(x) = 0, \quad (2)$$

where $w_i(x, t)$ is the transverse displacement field of the i -th beam. The i -th beam flexural stiffness $E_i I_i$ is assumed to be constant. The initial conditions given by w_{i0} and \dot{w}_{i0} represent the initial displacement and velocity fields, respectively.

The governing equations of transverse vibrations may be modified by non-dimensionalizing the spatial variable and the transverse displacement; the corresponding non-dimensional quantities are, respectively, denoted by ξ and \tilde{w}_i ,

$$x = L\xi, w_i = L\tilde{w}_i. \quad (3)$$

The modified governing equation for transverse vibrations for the i -th beam is given as follows:

$$\begin{aligned} \frac{E_i I_i}{L^3} \frac{\partial^4 \tilde{w}_i}{\partial \xi^4} + \frac{P_i}{L} \frac{\partial^2 \tilde{w}_i}{\partial \xi^2} + \frac{L\mu}{4} \left(\frac{\partial^2 \tilde{w}_1}{\partial t^2} + \frac{\partial^2 \tilde{w}_2}{\partial t^2} \right) \\ + L\rho_i A_i \frac{\partial^2 \tilde{w}_i}{\partial t^2} + (-1)^{i-1} Lk_L (\tilde{w}_1 - \tilde{w}_2) \\ + (-1)^{i-1} L^3 k_{NL} (\tilde{w}_1 - \tilde{w}_2)^3 = f_i. \end{aligned} \quad (4)$$

Referring to the Bernoulli–Fourier method, the i -th beam transverse displacement can be expressed in accordance with the modal expansion principle as a linear combination of modal coordinates \tilde{u}_{in} ,³⁷

$$\tilde{w}_i(\xi, t) = \sum_{n=1}^{+\infty} \varphi_n(\xi) \tilde{u}_n(t); \quad i = 1, 2, \quad (5)$$

where φ_n is the n -th mode shape function.

From here, two different cases are investigated according to the load type: the first is the case of fixed harmonic excitations (concentrated and uniformly distributed loads), and the second is the case of constant moving concentrated loads.

A. Case of fixed harmonic loads

In this case of a double-beam system transversally loaded with fixed concentrated or uniformly distributed harmonic excitations, the applied transverse forces are assumed to be given as products of two functions, each depending on one of the two independent variables,

$$f_i(\xi, t) = k_i(\xi)g_i(t); \quad i = 1, 2. \quad (6)$$

The relationships of Eqs. (5) and (6) are introduced in Eq. (4). The obtained equation is multiplied by the mode shape function φ_m and integrated with respect to ξ from 0 to 1; this procedure, referred to as the Bubnov–Galerkin method, enables the transformation of a PDE into an ODE,

$$\begin{aligned} \int_0^1 \sum_{n=1}^{+\infty} \left[\frac{E_i I_i}{L^3} \frac{d^4 \varphi_n(\xi)}{d\xi^4} \tilde{u}_{in}(t) + \frac{P_i}{L} \frac{d^2 \varphi_n(\xi)}{d\xi^2} \tilde{u}_{in}(t) \right. \\ + \frac{L\mu}{4} \left(\frac{d^2 \tilde{u}_{1n}(t)}{dt^2} + \frac{d^2 \tilde{u}_{2n}(t)}{dt^2} \right) \varphi_n(\xi) + L\rho_i A_i \frac{d^2 \tilde{u}_{in}(t)}{dt^2} \varphi_n(\xi) \\ + (-1)^{i-1} Lk_L (\tilde{u}_{1n}(t) - \tilde{u}_{2n}(t)) \varphi_n(\xi) \\ + (-1)^{i-1} L^3 k_{NL} (\tilde{u}_{1n}(t) - \tilde{u}_{2n}(t))^3 \varphi_n^3(\xi) \left. \right] \varphi_m(\xi) d\xi \\ = \int_0^1 k_i(\xi) g_i(t) \varphi_m(\xi) d\xi. \end{aligned} \quad (7)$$

The mode shape function φ_l may be defined as a function of $a_l \xi$; φ_l and its s -th derivative (s being an even number) with respect to ξ are written as follows:

$$\varphi_l(\xi) := h(a_l \xi), \quad \frac{d^s \varphi_l(\xi)}{d\xi^s} = \Gamma(a_l, s) \varphi_l(\xi), \quad (8)$$

where the function h depends on the boundary conditions. With the adopted boundary conditions, h is a sine function and the number a_l is equal to $l\pi$, where l is the mode number. If s is equal to $2p$, $\Gamma(a_l, s)$ is equal to $(-1)^p a_l^{2p}$. Γ is a function introduced to define the derivative of the mode shape function; it represents an eigen value of the operator $\frac{d^s}{d\xi^s}$. The equation corresponding to the n -th mode is given in the following equation:

$$\begin{aligned} \frac{d^2 \tilde{u}_{in}(t)}{dt^2} + \frac{\mu}{4\rho_i A_i} \left(\frac{d^2 \tilde{u}_{1n}(t)}{dt^2} + \frac{d^2 \tilde{u}_{2n}(t)}{dt^2} \right) \\ + \frac{\left(\frac{E_i I_i}{L^3} \Gamma(a_n, 4) + \frac{P_i}{L} \Gamma(a_n, 2) \right)}{L\rho_i A_i} \tilde{u}_{in}(t) \\ + \frac{(-1)^{i-1} k_L}{\rho_i A_i} (\tilde{u}_{1n}(t) - \tilde{u}_{2n}(t)) \\ + \frac{(-1)^{i-1} L^2 k_{NL} \int_0^1 \varphi_n^4(\xi) d\xi}{\rho_i A_i \int_0^1 \varphi_n^2(\xi) d\xi} (\tilde{u}_{1n}(t) - \tilde{u}_{2n}(t))^3 \\ = \frac{\int_0^1 k_i(\xi) \varphi_n(\xi) d\xi}{L\rho_i A_i \int_0^1 \varphi_n^2(\xi) d\xi} g_i(t). \end{aligned} \quad (9)$$

B. Case of moving concentrated loads

In the case of constant concentrated loads of magnitudes g_i , moving with constant speeds v_i , the exciting terms are defined with the Dirac delta function δ as follows:

$$f_i(\xi, t) = \frac{1}{L} \delta\left(\xi - \frac{v_i t}{L}\right) g_i; \quad i = 1, 2. \quad (10)$$

The relationships of Eqs. (5) and (10) are introduced in Eq. (4). The obtained equation is multiplied by the mode shape function φ_m and integrated with respect to ξ from 0 to 1; the equation corresponding to the n-th mode in the case of moving concentrated loads is given as follows:

$$\begin{aligned} \frac{d^2 \bar{u}_{i_n}(t)}{dt^2} + \frac{\mu}{4\rho_i A_i} \left(\frac{d^2 \bar{u}_{1_n}(t)}{dt^2} + \frac{d^2 \bar{u}_{2_n}(t)}{dt^2} \right) + \frac{\left(\frac{E_i I_i}{L^3} \Gamma(a_n, 4) + \frac{P_i}{L} \Gamma(a_n, 2) \right)}{L \rho_i A_i} \bar{u}_{i_n}(t) + \frac{(-1)^{i-1} k_L}{\rho_i A_i} (\bar{u}_{1_n}(t) - \bar{u}_{2_n}(t)) \\ + \frac{(-1)^{i-1} L^2 k_{NL} \int_0^1 \varphi_n^4(\xi) d\xi}{\rho_i A_i \int_0^1 \varphi_n^2(\xi) d\xi} (\bar{u}_{1_n}(t) - \bar{u}_{2_n}(t))^3 = \frac{\int_0^1 \delta\left(\xi - \frac{v_i}{L} t\right) \varphi_n(\xi) d\xi}{L^2 \rho_i A_i \int_0^1 \varphi_n^2(\xi) d\xi} g_i. \end{aligned} \tag{11}$$

C. Modified forms of equations of motion

The Bubnov–Galerkin technique allows the construction of a system of ODEs whose unknowns are the functions \bar{u}_{1_n} and \bar{u}_{2_n} . The system of ODEs is given as follows:

$$\begin{cases} \frac{d^2 \bar{u}_{1_n}}{dt^2} + \alpha_{11} \left(\frac{d^2 \bar{u}_{1_n}}{dt^2} + \frac{d^2 \bar{u}_{2_n}}{dt^2} \right) + \alpha_{12} \bar{u}_{1_n} + \alpha_{13} (\bar{u}_{1_n} - \bar{u}_{2_n}) + \alpha_{14} (\bar{u}_{1_n} - \bar{u}_{2_n})^3 = \alpha_{15} g_1, \\ \frac{d^2 \bar{u}_{2_n}}{dt^2} + \alpha_{21} \left(\frac{d^2 \bar{u}_{1_n}}{dt^2} + \frac{d^2 \bar{u}_{2_n}}{dt^2} \right) + \alpha_{22} \bar{u}_{2_n} + \alpha_{23} (\bar{u}_{1_n} - \bar{u}_{2_n}) + \alpha_{24} (\bar{u}_{1_n} - \bar{u}_{2_n})^3 = \alpha_{25} g_2, \end{cases} \tag{12}$$

where the coefficients α_{ij} ($i = 1, 2; j = 1, \dots, 5$) are given in the following equation:

$$\begin{aligned} \alpha_{i1} = \frac{\mu}{4\rho_i A_i}, \quad \alpha_{i2} = \frac{\frac{E_i I_i}{L^3} \Gamma(a_n, 4) + \frac{P_i}{L} \Gamma(a_n, 2)}{L \rho_i A_i}, \\ \alpha_{i3} = \frac{(-1)^{i-1} k_L}{\rho_i A_i}, \quad \alpha_{i4} = \frac{(-1)^{i-1} L^2 k_{NL} \int_0^1 \varphi_n^4(\xi) d\xi}{\rho_i A_i \int_0^1 \varphi_n^2(\xi) d\xi}, \tag{13} \\ \alpha_{i5} = \begin{cases} \frac{\int_0^1 k_i(\xi) \varphi_n(\xi) d\xi}{L \rho_i A_i \int_0^1 \varphi_n^2(\xi) d\xi}, & \text{for fixed loads,} \\ \frac{\int_0^1 \delta\left(\xi - \frac{v_i}{L} t\right) \varphi_n(\xi) d\xi}{L^2 \rho_i A_i \int_0^1 \varphi_n^2(\xi) d\xi}, & \text{for moving loads.} \end{cases} \end{aligned}$$

Using the definition of the Dirac delta function, the coefficients α_{i5} for moving loads are given as

$$\alpha_{i5} = \begin{cases} \frac{\varphi_n\left(\frac{v_i}{L} t\right)}{L^2 \rho_i A_i \int_0^1 \varphi_n^2(\xi) d\xi}, & \text{if } \frac{v_i}{L} t \in (0, 1), \\ 0, & \text{if } \frac{v_i}{L} t \notin [0, 1]. \end{cases} \tag{14}$$

The initial conditions corresponding to the n-th mode are derived as shown in the following equation:

$$\bar{u}_{i_n}(0) = \frac{\int_0^1 \bar{w}_{i0}(\xi) \varphi_n(\xi) d\xi}{\int_0^1 \varphi_n^2(\xi) d\xi}, \quad \dot{\bar{u}}_{i_n}(0) = \frac{\int_0^1 \dot{\bar{w}}_{i0}(\xi) \varphi_n(\xi) d\xi}{\int_0^1 \varphi_n^2(\xi) d\xi} = 0. \tag{15}$$

For the next step in the modification of the system of equations, we introduce two unknown functions denoted by \bar{u}_n and \bar{v}_n , given as follows:

$$\bar{u}_n = \bar{u}_{1_n} - \bar{u}_{2_n}, \quad \bar{v}_n = \bar{u}_{1_n} + \bar{u}_{2_n}. \tag{16}$$

The system of equations to be solved is then expressed as

$$\begin{cases} \frac{\partial^2 \bar{u}_n}{\partial t^2} + \sigma_{11} \bar{u}_n + \sigma_{12} \bar{v}_n + \sigma_{13} \bar{u}_n^3 = \sigma_{14} g_1 + \sigma_{15} g_2, \\ \frac{\partial^2 \bar{v}_n}{\partial t^2} + \sigma_{21} \bar{u}_n + \sigma_{22} \bar{v}_n + \sigma_{23} \bar{u}_n^3 = \sigma_{24} g_1 + \sigma_{25} g_2, \end{cases} \tag{17}$$

where the coefficients σ_{1j} and σ_{2j} ($j = 1, 2, 3, 4, 5$) are given in the following equations, respectively,

$$\begin{aligned} \sigma_{11} = \frac{0.5(\alpha_{12} + \alpha_{22}) + \alpha_{13} - \alpha_{23} + \alpha_{11}(\alpha_{22} - 2\alpha_{23}) + \alpha_{21}(\alpha_{12} + 2\alpha_{13})}{1 + \alpha_{11} + \alpha_{21}}, \\ \sigma_{12} = \frac{0.5\alpha_{12}(1 + 2\alpha_{21}) - 0.5\alpha_{22}(1 + 2\alpha_{11})}{1 + \alpha_{11} + \alpha_{21}}, \quad \sigma_{13} = \frac{\alpha_{14}(1 + 2\alpha_{21}) - \alpha_{24}(1 + 2\alpha_{11})}{1 + \alpha_{11} + \alpha_{21}}, \tag{18} \\ \sigma_{14} = \frac{\alpha_{15}(1 + 2\alpha_{21})}{1 + \alpha_{11} + \alpha_{21}}, \quad \sigma_{15} = \frac{-\alpha_{25}(1 + 2\alpha_{11})}{1 + \alpha_{11} + \alpha_{21}}, \end{aligned}$$

14 September 2023 13:11:11

$$\begin{aligned} \sigma_{21} &= \frac{0.5(\alpha_{12} - \alpha_{22}) + \alpha_{13} + \alpha_{23}}{1 + \alpha_{11} + \alpha_{21}}, & \sigma_{22} &= \frac{0.5(\alpha_{12} + \alpha_{22})}{1 + \alpha_{11} + \alpha_{21}}, \\ \sigma_{23} &= \frac{\alpha_{14} + \alpha_{24}}{1 + \alpha_{11} + \alpha_{21}}, & \sigma_{24} &= \frac{\alpha_{15}}{1 + \alpha_{11} + \alpha_{21}}, \\ \sigma_{25} &= \frac{\alpha_{25}}{1 + \alpha_{11} + \alpha_{21}}. \end{aligned} \tag{19}$$

It is guaranteed that the coefficients σ_{ij} are real numbers for every value of each of the independent variables, since the number $1 + \alpha_{11} + \alpha_{21}$ is always greater or equal to 1 (equal to 1 when the mass per unit length of the inner layer is disregarded).

III. SOLUTION OF THE SYSTEM OF EQUATIONS USING THE HAM

A. Preliminary work

A further modification of the system of ODEs to be solved concerns the non-dimensionalization of equations with respect to the temporal variable. The procedure differs according to whether loads are fixed or moving.

In the case of a fixed harmonic excitation characterized by the frequency ω , we introduce a dimensionless time denoted by τ , given as follows:

$$\tau = \omega t. \tag{20}$$

The system of equations to be solved is derived as in the following equation:

$$\begin{cases} \omega^2 \frac{d^2 \tilde{u}_n}{d\tau^2} + \sigma_{11} \tilde{u}_n + \sigma_{12} \tilde{v}_n + \sigma_{13} \tilde{u}_n^3 = g, \\ \omega^2 \frac{d^2 \tilde{v}_n}{d\tau^2} + \sigma_{21} \tilde{u}_n + \sigma_{22} \tilde{v}_n + \sigma_{23} \tilde{u}_n^3 = h, \end{cases} \tag{21}$$

where g and h are given as follows

$$g(\tau) = \sigma_{14} g_1(\tau) + \sigma_{15} g_2(\tau), \quad h(\tau) = \sigma_{24} g_1(\tau) + \sigma_{25} g_2(\tau), \tag{22}$$

with the initial conditions given as follows:

$$\begin{aligned} \tilde{u}_n(0) = \dot{\tilde{u}}_n(0) = \tilde{u}_{n0}^o, & \quad \left. \frac{d\tilde{u}_n}{d\tau} \right|_{t=0} = 0, \\ \tilde{v}_n(0) = \dot{\tilde{v}}_n(0) = \tilde{v}_{n0}^o, & \quad \left. \frac{d\tilde{v}_n}{d\tau} \right|_{t=0} = 0. \end{aligned} \tag{23}$$

Regarding the case of constant moving forces, we consider the mode shape function related to the chosen boundary conditions,

$$\varphi_n(\xi) = \cos\left(n\pi\xi - \frac{\pi}{2}\right). \tag{24}$$

A cosine form is adopted to define the mode shape function, instead of the original sine form, to comply with the solution structure built with cosine functions. The time scale is modified, but results corresponding to the same time point in the cases of sine and cosine forms remain the same since the two functions are mathematically the same despite being written in two different forms. The corresponding dimensionless temporal variable is defined considering the expression $\varphi_n(\frac{\nu_i}{L}t)$ stemming from the integration of the Dirac delta function,

$$\tau_n^* = \frac{n\pi\nu_i}{L}t - \pi/2 = \omega_n^*t - \pi/2. \tag{25}$$

The system of equations to be solved is derived as in the following equation:

$$\begin{cases} \omega_n^{*2} \frac{d^2 \tilde{u}_n}{d\tau_n^{*2}} + \sigma_{11} \tilde{u}_n + \sigma_{12} \tilde{v}_n + \sigma_{13} \tilde{u}_n^3 = g, \\ \omega_n^{*2} \frac{d^2 \tilde{v}_n}{d\tau_n^{*2}} + \sigma_{21} \tilde{u}_n + \sigma_{22} \tilde{v}_n + \sigma_{23} \tilde{u}_n^3 = h, \end{cases} \tag{26}$$

where g and h are given as follows:

$$g(\tau_n^*) = \sigma_{14}(\tau_n^*)g_1 + \sigma_{15}(\tau_n^*)g_2, \quad h(\tau_n^*) = \sigma_{24}(\tau_n^*)g_1 + \sigma_{25}(\tau_n^*)g_2. \tag{27}$$

The variable τ_n^* being dependent on the mode order n , is only used in the algorithm development; solutions will be presented as functions of $\tau^* = \frac{n\nu_i}{L}t$.

B. Application of the HAM

The HAM is now applied to first compute the time-dependent unknown functions \tilde{u}_n and \tilde{v}_n ; afterward, the time-dependent parts \tilde{u}_{1n} and \tilde{u}_{2n} of the transverse vibrations will be deduced in order to construct the dynamic vibration functions using the modal superposition principle.

For each of the equations of the system of ODEs, a function denoted by \mathcal{H} and named the homotopy function is introduced. \mathcal{H} is a function of the approximate value and depends on the embedding parameter or the homotopy-parameter q ($q \in [0, 1]$). In the context of the HAM, the approximate functions of \tilde{u}_n and \tilde{v}_n are denoted by \tilde{u}_n and \tilde{v}_n , respectively; the homotopy functions are expressed as

$$\begin{aligned} \mathcal{H}_1(\tilde{u}_n; q) &:= (1 - q)\mathcal{L}_1[\tilde{u}_n(\tau; q) - \tilde{u}_{n0}(\tau)] - c_{01}qH_1\mathcal{N}_1[\tilde{u}_n(\tau; q)], \\ \mathcal{H}_2(\tilde{v}_n; q) &:= (1 - q)\mathcal{L}_2[\tilde{v}_n(\tau; q) - \tilde{v}_{n0}(\tau)] - c_{02}qH_2\mathcal{N}_2[\tilde{v}_n(\tau; q)]. \end{aligned} \tag{28}$$

Subsequently, we define the homotopy equations \mathcal{E}_i from each of the homotopy functions; \mathcal{E}_i represents the families of equations that can be generated for different values of q ,

$$\begin{aligned} \mathcal{E}_1(q) &: (1 - q)\mathcal{L}_1[\tilde{u}_n(\tau; q) - \tilde{u}_{n0}(\tau)] - c_{01}qH_1\mathcal{N}_1[\tilde{u}_n(\tau; q)] = 0, \\ \mathcal{E}_2(q) &: (1 - q)\mathcal{L}_2[\tilde{v}_n(\tau; q) - \tilde{v}_{n0}(\tau)] - c_{02}qH_2\mathcal{N}_2[\tilde{v}_n(\tau; q)] = 0. \end{aligned} \tag{29}$$

In \mathcal{H}_i and \mathcal{E}_i , \mathcal{L}_i represent the linear operators corresponding to appropriate linear partial differential equations; \mathcal{N}_i are the nonlinear operators representing the nonlinear partial differential equations to be solved, in which the unknowns \tilde{u}_n and \tilde{v}_n are substituted with their approximations \tilde{u}_n and \tilde{v}_n , respectively, for a certain value of the homotopy parameter. Assuming that the linear operators have been appropriately chosen, the convergence of the algorithm to be built depends on the choice of the initial guesses $\tilde{u}_{n0}(\tau)$ and $\tilde{v}_{n0}(\tau)$, on the convergence-control parameters c_{0i} , and, to some extent, on the auxiliary functions H_i .

The expressions in Eq. (29) are referred to as zeroth-order deformation equations. They express the continuous deformation of the solutions to the problem from the initial guesses $\tilde{u}_{n0}(\tau)$ and $\tilde{v}_{n0}(\tau)$ as solutions to linear equations ($q = 0$) represented by the linear operators to $\tilde{u}_n(\tau; 1)$ and $\tilde{v}_n(\tau; 1)$, respectively, as solutions to the nonlinear equations to be solved ($q = 1$) represented by the nonlinear operators.

The nonlinear operators deduced from the system of equations to be solved and the chosen linear operators are given in Eqs. (30) and (31), respectively,

$$\mathcal{N}_1[\tilde{u}_n(\tau; q)] = \omega^2 \frac{d^2 \tilde{u}_n(\tau; q)}{d\tau^2} + \sigma_{11} \tilde{u}_n(\tau; q) + \sigma_{12} \tilde{v}_n(\tau; q) + \sigma_{13} \tilde{u}_n^3(\tau; q) - \tilde{g}(\tau; q), \tag{30}$$

$$\mathcal{N}_2[\tilde{v}_n(\tau; q)] = \omega^2 \frac{d^2 \tilde{v}_n(\tau; q)}{d\tau^2} + \sigma_{21} \tilde{u}_n(\tau; q) + \sigma_{22} \tilde{v}_n(\tau; q) + \sigma_{23} \tilde{u}_n^3(\tau; q) - \tilde{h}(\tau; q),$$

$$\begin{aligned} \mathcal{L}_1[\tilde{u}_n(\tau; q)] &= \omega^2 \left(\frac{d^2 \tilde{u}_n(\tau; q)}{d\tau^2} + \tilde{u}_n(\tau; q) \right), \\ \mathcal{L}_2[\tilde{v}_n(\tau; q)] &= \omega^2 \left(\frac{d^2 \tilde{v}_n(\tau; q)}{d\tau^2} + \tilde{v}_n(\tau; q) \right). \end{aligned} \tag{31}$$

The approximate solutions within the framework of the HAM are given as follows:

$$\tilde{u}_n(\tau; q) \sim \sum_{m=0}^{+\infty} \tilde{u}_{n_m}(\tau) q^m \text{ and } \tilde{v}_n(\tau; q) \sim \sum_{m=0}^{+\infty} \tilde{v}_{n_m}(\tau) q^m, \tag{32}$$

where the unknown functions \tilde{u}_{n_m} and \tilde{v}_{n_m} are obtained as follows:

$$\begin{aligned} \tilde{u}_{n_m}(\tau) &= \frac{1}{m!} \left. \frac{\partial^m \tilde{u}_n(\tau; q)}{\partial q^m} \right|_{q=0} = \mathcal{D}_{1_m}[\tilde{u}_n(\tau; q)], \\ \tilde{v}_{n_m}(\tau) &= \frac{1}{m!} \left. \frac{\partial^m \tilde{v}_n(\tau; q)}{\partial q^m} \right|_{q=0} = \mathcal{D}_{2_m}[\tilde{v}_n(\tau; q)]. \end{aligned} \tag{33}$$

It is assumed that g and h are made of different components g_m and h_m , respectively, and are written as an infinite series of functions,

$$\tilde{g}(\tau; q) \sim \sum_{m=0}^{+\infty} g_m(\tau) q^m, \quad \tilde{h}(\tau; q) \sim \sum_{m=0}^{+\infty} h_m(\tau) q^m. \tag{34}$$

We can now build higher-order deformation equations. The substitution of the approximate unknown functions with their infinite series representations given in Eq. (32) in the left-hand side of Eq. (29) yields

$$\begin{aligned} (1-q)\mathcal{L}_1[\tilde{u}_n(\tau; q) - \tilde{u}_{n_0}(\tau)] &= \sum_{m=1}^{+\infty} \mathcal{L}_1[\tilde{u}_{n_m}(\tau) - \chi_m \tilde{u}_{n_{m-1}}(\tau)] q^m, \\ (1-q)\mathcal{L}_2[\tilde{v}_n(\tau; q) - \tilde{v}_{n_0}(\tau)] &= \sum_{m=1}^{+\infty} \mathcal{L}_2[\tilde{v}_{n_m}(\tau) - \chi_m \tilde{v}_{n_{m-1}}(\tau)] q^m, \end{aligned} \tag{35}$$

$$\chi_m = \begin{cases} 0, & m \leq 1, \\ 1, & m > 1. \end{cases} \tag{36}$$

Performing the same substitution at the right-hand side of Eq. (29) yields the following equation:

$$q\mathcal{N}_1[\tilde{u}_n(\tau; q)] = \sum_{m=1}^{+\infty} \delta_{1_m}^{(n)} q^m, \quad q\mathcal{N}_2[\tilde{v}_n(\tau; q)] = \sum_{m=1}^{+\infty} \delta_{2_m}^{(n)} q^m, \tag{37}$$

where $\delta_{1_m}^{(n)}$ and $\delta_{2_m}^{(n)}$ are given as follows:

$$\begin{aligned} \delta_{1_m}^{(n)} &= \omega^2 \frac{d^2 \tilde{u}_{n_{m-1}}}{d\tau^2} + \sigma_{11} \tilde{u}_{n_{m-1}} + \sigma_{12} \tilde{v}_{n_{m-1}} \\ &\quad + \sigma_{13} \sum_{k=0}^{m-1} \sum_{j=0}^k \tilde{u}_{n_{m-k-1}} \tilde{u}_{n_{k-j}} \tilde{u}_{n_j} - g_{m-1}, \end{aligned} \tag{38}$$

$$\begin{aligned} \delta_{2_m}^{(n)} &= \omega^2 \frac{d^2 \tilde{v}_{n_{m-1}}}{d\tau^2} + \sigma_{21} \tilde{u}_{n_{m-1}} + \sigma_{22} \tilde{v}_{n_{m-1}} \\ &\quad + \sigma_{23} \sum_{k=0}^{m-1} \sum_{j=0}^k \tilde{u}_{n_{m-k-1}} \tilde{u}_{n_{k-j}} \tilde{u}_{n_j} - h_{m-1}. \end{aligned}$$

Finally, the m -th order deformation equations are given as follows:

$$\mathcal{L}_1[\tilde{u}_{n_m}(\tau) - \chi_m \tilde{u}_{n_{m-1}}(\tau)] = c_{0_1} H_1 \delta_{1_m}^{(n)}$$

and

$$\mathcal{L}_2[\tilde{v}_{n_m}(\tau) - \chi_m \tilde{v}_{n_{m-1}}(\tau)] = c_{0_2} H_2 \delta_{2_m}^{(n)}, \tag{39}$$

with the initial conditions

$$\tilde{u}_{n_m}(\tau = 0) = 0, \quad \left. \frac{d\tilde{u}_{n_m}}{d\tau} \right|_{\tau=0} = 0, \quad \tilde{v}_{n_m}(\tau = 0) = 0, \quad \left. \frac{d\tilde{v}_{n_m}}{d\tau} \right|_{\tau=0} = 0. \tag{40}$$

The next step in the procedure consists of the calculation of the successive values of the coefficients $\tilde{u}_{n_k}(\tau)$ and $\tilde{v}_{n_k}(\tau)$ ($k = 0, 1, \dots, M$) to construct the M -th-order homotopy-approximation solutions as given in Eq. (41) under the consideration that all the conditions are fulfilled so that the convergence of the series given in Eq. (32) for $q = 1$ is guaranteed,

$$\tilde{u}_n(\tau) \sim \sum_{m=0}^M \tilde{u}_{n_m}(\tau) \text{ and } \tilde{v}_n(\tau) \sim \sum_{m=0}^M \tilde{v}_{n_m}(\tau). \tag{41}$$

The initial guesses have to comply with the initial conditions of Eq. (23); they are chosen as follows:

$$\tilde{u}_{n_0}(\tau) = a_1 + b_1 \cos \tau \text{ and } \tilde{v}_{n_0}(\tau) = a_2 + b_2 \cos \tau; \quad b_1, b_2 \neq 0, \tag{42}$$

where the numbers b_1 and b_2 are such that

$$b_1 = \tilde{u}_n^0 - a_1, \quad b_2 = \tilde{v}_n^0 - a_2. \tag{43}$$

The numbers a_1 and a_2 are chosen with a relatively straightforward procedure that will be presented later as one way of guaranteeing convergence.

The first-order deformation equations are given as follows:

$$\begin{aligned} \mathcal{L}_1[\tilde{u}_{n_1}(\tau)] &= c_{0_1} H_1 \delta_{1_1}^{(n)} \\ &= c_{0_1} H_1 \left(\omega^2 \frac{d^2 \tilde{u}_{n_0}}{d\tau^2} + \sigma_{11} \tilde{u}_{n_0} + \sigma_{12} \tilde{v}_{n_0} + \sigma_{13} \tilde{u}_{n_0}^3 - g_0 \right), \\ \mathcal{L}_2[\tilde{v}_{n_1}(\tau)] &= c_{0_2} H_2 \delta_{2_1}^{(n)} \\ &= c_{0_2} H_2 \left(\omega^2 \frac{d^2 \tilde{v}_{n_0}}{d\tau^2} + \sigma_{21} \tilde{u}_{n_0} + \sigma_{22} \tilde{v}_{n_0} + \sigma_{23} \tilde{u}_{n_0}^3 - h_0 \right). \end{aligned} \tag{44}$$

It is assumed that $H_1(\tau) = H_2(\tau) = 1$ for the sake of simplicity and g_0 and h_0 are such that

$$g_0 = \lambda_{1_0} \cos \tau, h_0 = \lambda_{2_0} \cos \tau. \tag{45}$$

The right-hand sides of the first-order deformation equations are developed and rearranged as follows:

$$\begin{aligned} c_{0_1} \delta_{1_1}^{(n)} &= \Delta_{1_{1,0}}^{(n)} + \Delta_{1_{1,1}}^{(n)} \cos \tau + \Delta_{1_{1,2}}^{(n)} \cos 2\tau + \Delta_{1_{1,3}}^{(n)} \cos 3\tau, \\ c_{0_2} \delta_{2_1}^{(n)} &= \Delta_{2_{1,0}}^{(n)} + \Delta_{2_{1,1}}^{(n)} \cos \tau + \Delta_{2_{1,2}}^{(n)} \cos 2\tau + \Delta_{2_{1,3}}^{(n)} \cos 3\tau, \end{aligned} \tag{46}$$

Where coefficients $\Delta_{k_{1,j}}^{(n)}$ ($k = 1, 2$ and $j = 0, 1, 2, 3$) are given in the following equation:

$$\begin{aligned} \Delta_{k_{1,0}}^{(n)} &= c_{0_k} (\sigma_{k1} a_1 + \sigma_{k2} a_2 + \sigma_{k3} a_1^3 + 1.5 \sigma_{k3} a_1 b_1^2), \\ \Delta_{k_{1,1}}^{(n)} &= c_{0_k} (-\omega^2 b_k + \sigma_{k1} b_1 + \sigma_{k2} b_2 + 0.75 \sigma_{k3} b_1^3 + 3 \sigma_{k3} a_1^2 b_1 - \lambda_{k_0}), \\ \Delta_{k_{1,2}}^{(n)} &= 1.5 c_{0_k} \sigma_{k3} a_1 b_1^2, \Delta_{k_{1,3}}^{(n)} = 0.25 c_{0_k} \sigma_{k3} b_1^3. \end{aligned} \tag{47}$$

In order to avoid the so-called secular terms in the solutions, the coefficients $\Delta_{1_{1,1}}^{(n)}$ and $\Delta_{2_{1,1}}^{(n)}$ should be set to zero. Such conditions provide a way of calculating the lower and higher natural frequencies of the system considering free conditions ($\lambda_{1_0} = \lambda_{2_0} = 0$),

$$\begin{aligned} \Delta_{1_{1,1}}^{(n)} = 0 &\implies \omega_{0_1}^{(n)} = \sqrt{\sigma_{11} + \sigma_{12} \frac{b_2}{b_1} + 0.75 \sigma_{13} b_1^2 + 3 \sigma_{13} a_1^2}, \\ \Delta_{2_{1,1}}^{(n)} = 0 &\implies \omega_{0_2}^{(n)} = \sqrt{\sigma_{21} \frac{b_1}{b_2} + \sigma_{22} + 0.75 \sigma_{23} \frac{b_1^3}{b_2} + 3 \sigma_{23} a_1^2 \frac{b_1}{b_2}}. \end{aligned} \tag{48}$$

One of the advantages of the HAM is the great freedom with which some parameters are chosen. It is, however, necessary to have the guarantee of convergence. One of the ways of guaranteeing convergence is through a good choice of the initial guess. The squared residuals E_m , corresponding to the m -th iteration are calculated for this purpose. For the zero-th order approximation, we have the following equations:

$$\begin{aligned} E_{0_1}(a_1, a_2) &= \frac{1}{2\pi} \int_0^{2\pi} \{ \mathcal{N}_1[\tilde{u}_{n_0}(\tau)] \}^2 d\tau \\ &= \frac{1}{c_{0_1}^2} (\Delta_{1_{1,0}}^{(n)2} + 0.5 \Delta_{1_{1,2}}^{(n)2} + 0.5 \Delta_{1_{1,3}}^{(n)2}), \\ E_{0_2}(a_1, a_2) &= \frac{1}{2\pi} \int_0^{2\pi} \{ \mathcal{N}_2[\tilde{v}_{n_0}(\tau)] \}^2 d\tau \\ &= \frac{1}{c_{0_2}^2} (\Delta_{2_{1,0}}^{(n)2} + 0.5 \Delta_{2_{1,2}}^{(n)2} + 0.5 \Delta_{2_{1,3}}^{(n)2}). \end{aligned} \tag{49}$$

To guarantee convergence, the numbers a_1 and a_2 are chosen so that at least one among the functions E_{0_1} and E_{0_2} and the norm of the vector (E_{0_1}, E_{0_2}) is minimal. The corresponding values of a_1 and a_2 are denoted by \hat{a}_1 and \hat{a}_2 , respectively [\hat{b}_1 and \hat{b}_2 are deduced using Eq. (43)].

The solutions of the deformation equations [Eq. (39)] are constructed as follows:

$$\begin{aligned} \tilde{u}_{n_m}(\tau) - \chi_m \tilde{u}_{n_{m-1}}(\tau) &= \tilde{u}_{n_m}^s(\tau) + \tilde{u}_{n_m}^h(\tau), \\ \tilde{v}_{n_m}(\tau) - \chi_m \tilde{v}_{n_{m-1}}(\tau) &= \tilde{v}_{n_m}^s(\tau) + \tilde{v}_{n_m}^h(\tau), \end{aligned} \tag{50}$$

where $\tilde{u}_{n_m}^s(\tau)$ and $\tilde{v}_{n_m}^s(\tau)$ are special solutions of Eq. (39); $\tilde{u}_{n_m}^h(\tau)$ and $\tilde{v}_{n_m}^h(\tau)$ are the solutions of homogeneous equations as shown below:

$$\mathcal{L}_1[\tilde{u}_{n_m}^h(\tau)] = 0, \mathcal{L}_2[\tilde{v}_{n_m}^h(\tau)] = 0. \tag{51}$$

Considering the linear operators \mathcal{L}_1 and \mathcal{L}_2 , as given in Eq. (31), the solutions of the homogeneous equations are given as

$$\begin{aligned} \tilde{u}_{n_m}^h(\tau) &= C_{1_{m,1}}^{(n)} \cos \tau + C_{1_{m,2}}^{(n)} \sin \tau, \\ \tilde{v}_{n_m}^h(\tau) &= C_{2_{m,1}}^{(n)} \cos \tau + C_{2_{m,2}}^{(n)} \sin \tau. \end{aligned} \tag{52}$$

We set $C_{1_{m,2}}^{(n)} = C_{2_{m,2}}^{(n)} = 0$ to comply with the solution structure; the initial conditions in Eq. (40) enable the calculation of $C_{1_{m,1}}^{(n)}$ and $C_{2_{m,1}}^{(n)}$,

$$\begin{aligned} C_{1_{m,1}}^{(n)} &= -\chi_m \tilde{u}_{n_{m-1}}(0) - \tilde{u}_{n_m}^s(0), \\ C_{2_{m,1}}^{(n)} &= -\chi_m \tilde{v}_{n_{m-1}}(0) - \tilde{v}_{n_m}^s(0). \end{aligned} \tag{53}$$

Special solutions have the same structure as the right-hand side of Eq. (44), developed in Eq. (46),

$$\begin{aligned} \tilde{u}_{n_1}^s(\tau) &= \Psi_{1_{1,0}}^{(n)} + \Psi_{1_{1,2}}^{(n)} \cos 2\tau + \Psi_{1_{1,3}}^{(n)} \cos 3\tau, \\ \tilde{v}_{n_1}^s(\tau) &= \Psi_{2_{1,0}}^{(n)} + \Psi_{2_{1,2}}^{(n)} \cos 2\tau + \Psi_{2_{1,3}}^{(n)} \cos 3\tau. \end{aligned} \tag{54}$$

The coefficients $\Psi_{i,j}^{(n)}$ ($i = 1, 2; j = 0, 1, 2, 3$) are determined after incorporating the special solutions in Eqs. (44) and (53),

$$\Psi_{i,0}^{(n)} = \frac{1}{\omega^2} \Delta_{i,0}^{(n)}, \Psi_{i,2}^{(n)} = -\frac{1}{3\omega^2} \Delta_{i,2}^{(n)}, \Psi_{i,3}^{(n)} = -\frac{1}{8\omega^2} \Delta_{i,3}^{(n)}; i = 1, 2, \tag{55}$$

$$\begin{aligned} C_{1_{1,1}}^{(n)} &= -\tilde{u}_{n_1}^s(0) = -(\Psi_{1_{1,0}}^{(n)} + \Psi_{1_{1,2}}^{(n)} + \Psi_{1_{1,3}}^{(n)}) = \Psi_{1_{1,1}}^{(n)}, \\ C_{2_{1,1}}^{(n)} &= -\tilde{v}_{n_1}^s(0) = -(\Psi_{2_{1,0}}^{(n)} + \Psi_{2_{1,2}}^{(n)} + \Psi_{2_{1,3}}^{(n)}) = \Psi_{2_{1,1}}^{(n)}. \end{aligned} \tag{56}$$

The general solution for the first-order homotopy approximation ($m = 1$) can now be determined,

$$\begin{aligned} \tilde{u}_{n_1}(\tau) &= \Psi_{1_{1,0}}^{(n)} + \Psi_{1_{1,1}}^{(n)} \cos \tau + \Psi_{1_{1,2}}^{(n)} \cos 2\tau + \Psi_{1_{1,3}}^{(n)} \cos 3\tau, \\ \tilde{v}_{n_1}(\tau) &= \Psi_{2_{1,0}}^{(n)} + \Psi_{2_{1,1}}^{(n)} \cos \tau + \Psi_{2_{1,2}}^{(n)} \cos 2\tau + \Psi_{2_{1,3}}^{(n)} \cos 3\tau. \end{aligned} \tag{57}$$

Using the same procedure, the general solution for the first-order homotopy approximation in the case of a system subjected to moving loads is written as follows:

$$\begin{aligned} \tilde{u}_{n_1}(\tau_n^*) &= \Psi_{1_{1,0}}^{*(n)} + \Psi_{1_{1,1}}^{*(n)} \cos \tau_n^* + \Psi_{1_{1,2}}^{*(n)} \cos 2\tau_n^* + \Psi_{1_{1,3}}^{*(n)} \cos 3\tau_n^*, \\ \tilde{v}_{n_1}(\tau_n^*) &= \Psi_{2_{1,0}}^{*(n)} + \Psi_{2_{1,1}}^{*(n)} \cos \tau_n^* + \Psi_{2_{1,2}}^{*(n)} \cos 2\tau_n^* + \Psi_{2_{1,3}}^{*(n)} \cos 3\tau_n^*. \end{aligned} \tag{58}$$

At the second iteration, $\delta_{12}^{(n)}$ and $\delta_{22}^{(n)}$ are expressed as in the following equation, and the right-hand sides of Eq. (39) are developed as shown in Eq. (61):

$$\begin{aligned} \delta_{12}^{(n)} &= \omega^2 \frac{d^2 \bar{u}_{n1}}{d\tau^2} + \sigma_{11} \bar{u}_{n1} + \sigma_{12} \bar{v}_{n1} + 3\sigma_{13} \bar{u}_{n0}^2 \bar{u}_{n1} - g_1, \\ \delta_{22}^{(n)} &= \omega^2 \frac{d^2 \bar{v}_{n1}}{d\tau^2} + \sigma_{21} \bar{u}_{n1} + \sigma_{22} \bar{v}_{n1} + 3\sigma_{23} \bar{u}_{n0}^2 \bar{u}_{n1} - h_1, \end{aligned} \tag{59}$$

where g_1 and h_1 can be written as

$$g_1 = \lambda_{11} \cos \tau, \quad h_1 = \lambda_{21} \cos \tau. \tag{60}$$

The right-hand sides of the second-order deformation equations are developed and rearranged as follows:

$$\begin{aligned} c_{01} \delta_{12}^{(n)} &= \Delta_{1,0}^{(n)} + \Delta_{1,1}^{(n)} \cos \tau + \Delta_{1,2}^{(n)} \cos 2\tau + \Delta_{1,3}^{(n)} \cos 3\tau \\ &\quad + \Delta_{1,4}^{(n)} \cos 4\tau + \Delta_{1,5}^{(n)} \cos 5\tau, \\ c_{02} \delta_{22}^{(n)} &= \Delta_{2,0}^{(n)} + \Delta_{2,1}^{(n)} \cos \tau + \Delta_{2,2}^{(n)} \cos 2\tau + \Delta_{2,3}^{(n)} \cos 3\tau \\ &\quad + \Delta_{2,4}^{(n)} \cos 4\tau + \Delta_{2,5}^{(n)} \cos 5\tau. \end{aligned} \tag{61}$$

The coefficients $\Delta_{k,j}^{(n)}$ in Eq. (61) ($k = 1, 2$ and $j = 0, 1, \dots, 5$) are given in the following equation:

$$\begin{aligned} \Delta_{k,0}^{(n)} &= c_{0k} \left(\sigma_{k1} \Psi_{1,0}^{(n)} + \sigma_{k2} \Psi_{2,0}^{(n)} + 3\sigma_{k3} \eta_{1,0}^{(n)} \right), \\ \Delta_{k,1}^{(n)} &= c_{0k} \left(-\Psi_{k,1}^{(n)} \omega^2 + \sigma_{k1} \Psi_{1,1}^{(n)} + \sigma_{k2} \Psi_{2,1}^{(n)} + 3\sigma_{k3} \eta_{1,1}^{(n)} - \lambda_{k1} \right), \\ \Delta_{k,2}^{(n)} &= c_{0k} \left(-4\Psi_{k,2}^{(n)} \omega^2 + \sigma_{k1} \Psi_{1,2}^{(n)} + \sigma_{k2} \Psi_{2,2}^{(n)} + 3\sigma_{k3} \eta_{1,2}^{(n)} \right), \\ \Delta_{k,3}^{(n)} &= c_{0k} \left(-9\Psi_{k,3}^{(n)} \omega^2 + \sigma_{k1} \Psi_{1,3}^{(n)} + \sigma_{k2} \Psi_{2,3}^{(n)} + 3\sigma_{k3} \eta_{1,3}^{(n)} \right), \\ \Delta_{k,4}^{(n)} &= 3c_{0k} \sigma_{k3} \eta_{1,4}^{(n)}, \quad \Delta_{k,5}^{(n)} = 3c_{0k} \sigma_{k3} \eta_{1,5}^{(n)}, \end{aligned} \tag{62}$$

where the numbers $\eta_{1,j}^{(n)}$ ($j = 0, 1, \dots, 5$) are given as follows:

$$\begin{aligned} \eta_{1,0}^{(n)} &= \hat{a}_1^2 \Psi_{1,0}^{(n)} + 0.5 \hat{b}_1^2 \Psi_{1,0}^{(n)} + \hat{a}_1 \hat{b}_1 \Psi_{1,1}^{(n)} + 0.25 \hat{b}_1^2 \Psi_{1,2}^{(n)}, \\ \eta_{1,1}^{(n)} &= \hat{a}_1^2 \Psi_{1,1}^{(n)} + 2.25 \hat{b}_1^2 \Psi_{1,1}^{(n)} + 0.25 \hat{b}_1^2 \Psi_{1,3}^{(n)} + 2\hat{a}_1 \hat{b}_1 \Psi_{1,0}^{(n)} + \hat{a}_1 \hat{b}_1 \Psi_{1,2}^{(n)}, \\ \eta_{1,2}^{(n)} &= \hat{a}_1^2 \Psi_{1,2}^{(n)} + 0.5 \hat{b}_1^2 \Psi_{1,0}^{(n)} + \hat{a}_1 \hat{b}_1 \Psi_{1,1}^{(n)} + 0.5 \hat{b}_1^2 \Psi_{1,2}^{(n)} + \hat{a}_1 \hat{b}_1 \Psi_{1,3}^{(n)}, \\ \eta_{1,3}^{(n)} &= \hat{a}_1^2 \Psi_{1,3}^{(n)} + 0.75 \hat{b}_1^2 \Psi_{1,1}^{(n)} + 0.5 \hat{b}_1^2 \Psi_{1,3}^{(n)} + \hat{a}_1 \hat{b}_1 \Psi_{1,2}^{(n)}, \\ \eta_{1,4}^{(n)} &= 0.25 \hat{b}_1^2 \Psi_{1,2}^{(n)} + \hat{a}_1 \hat{b}_1 \Psi_{1,3}^{(n)}, \quad \eta_{1,5}^{(n)} = 0.25 \hat{b}_1^2 \Psi_{1,3}^{(n)}. \end{aligned} \tag{63}$$

The new lower and higher natural frequencies are again deduced considering free conditions ($\lambda_{11} = \lambda_{21} = 0$) and the condition that the solutions do not contain the so-called secular terms,

$$\begin{aligned} \Delta_{1,1}^{(n)} = 0 &\implies \omega_{11}^{(n)} = \sqrt{\sigma_{11} + \sigma_{12} \frac{\Psi_{2,1}^{(n)}}{\Psi_{1,1}^{(n)}} + \frac{3\sigma_{13} \eta_{1,1}^{(n)}}{\Psi_{1,1}^{(n)}}}, \\ \Delta_{2,1}^{(n)} = 0 &\implies \omega_{12}^{(n)} = \sqrt{\sigma_{21} \frac{\Psi_{1,1}^{(n)}}{\Psi_{2,1}^{(n)}} + \sigma_{22} + \frac{3\sigma_{23} \eta_{1,1}^{(n)}}{\Psi_{2,1}^{(n)}}}. \end{aligned} \tag{64}$$

The general solutions \bar{u}_{n2} and \bar{v}_{n2} at the second iteration are constructed from the homogeneous equations' solutions \bar{u}_{n2}^h and \bar{v}_{n2}^h and the special solutions \bar{u}_{n2}^s and \bar{v}_{n2}^s , respectively. The special solutions have to comply with the structure of Eq. (61); they are presented as developed in the following equation:

$$\begin{aligned} \bar{u}_{n2}^s(\tau) &= \Psi_{1,2,0}^{(n)} + \Psi_{1,2,2}^{(n)} \cos 2\tau + \Psi_{1,2,3}^{(n)} \cos 3\tau \\ &\quad + \Psi_{1,2,4}^{(n)} \cos 4\tau + \Psi_{1,2,5}^{(n)} \cos 5\tau, \\ \bar{v}_{n2}^s(\tau) &= \Psi_{2,2,0}^{(n)} + \Psi_{2,2,2}^{(n)} \cos 2\tau + \Psi_{2,2,3}^{(n)} \cos 3\tau \\ &\quad + \Psi_{2,2,4}^{(n)} \cos 4\tau + \Psi_{2,2,5}^{(n)} \cos 5\tau, \end{aligned} \tag{65}$$

where coefficients $\Psi_{i,j}^{(n)}$ ($i = 1, 2; j = 0, 1, \dots, 5$) are given as follows:

$$\begin{aligned} \Psi_{i,2,0}^{(n)} &= \frac{1}{\omega^2} \Delta_{i,2,0}^{(n)}, \quad \Psi_{i,2,2}^{(n)} = -\frac{1}{3\omega^2} \Delta_{i,2,2}^{(n)}, \quad \Psi_{i,2,3}^{(n)} = -\frac{1}{8\omega^2} \Delta_{i,2,3}^{(n)}, \\ \Psi_{i,2,4}^{(n)} &= -\frac{1}{15\omega^2} \Delta_{i,2,4}^{(n)}, \quad \Psi_{i,2,5}^{(n)} = -\frac{1}{24\omega^2} \Delta_{i,2,5}^{(n)}; \quad i = 1, 2. \end{aligned} \tag{66}$$

The homogeneous equations' solutions are given as

$$\bar{u}_{n2}^h(\tau) = C_{1,2,1}^{(n)} \cos \tau \quad \text{and} \quad \bar{v}_{n2}^h(\tau) = C_{2,2,1}^{(n)} \cos \tau, \tag{67}$$

with the two constants given as

$$\begin{aligned} C_{1,2,1}^{(n)} &= -\bar{u}_{n1}(0) - \bar{u}_{n2}^s(0) \quad \text{and} \quad C_{2,2,1}^{(n)} = -\bar{v}_{n1}(0) - \bar{v}_{n2}^s(0), \\ C_{1,2,1}^{(n)} &= -\left(\Psi_{1,1,0}^{(n)} + \Psi_{1,1,1}^{(n)} + \Psi_{1,1,2}^{(n)} + \Psi_{1,1,3}^{(n)} \right) \\ &\quad - \left(\Psi_{1,2,0}^{(n)} + \Psi_{1,2,2}^{(n)} + \Psi_{1,2,3}^{(n)} + \Psi_{1,2,4}^{(n)} + \Psi_{1,2,5}^{(n)} \right) = \Psi_{1,2,1}^{(n)}, \\ C_{2,2,1}^{(n)} &= -\left(\Psi_{2,1,0}^{(n)} + \Psi_{2,1,1}^{(n)} + \Psi_{2,1,2}^{(n)} + \Psi_{2,1,3}^{(n)} \right) \\ &\quad - \left(\Psi_{2,2,0}^{(n)} + \Psi_{2,2,2}^{(n)} + \Psi_{2,2,3}^{(n)} + \Psi_{2,2,4}^{(n)} + \Psi_{2,2,5}^{(n)} \right) = \Psi_{2,2,1}^{(n)}. \end{aligned} \tag{69}$$

Finally, the general solutions at the second iteration are derived as follows:

$$\begin{aligned} \bar{u}_{n2}(\tau) &= \Psi_{1,2,0}^{(n)} + \Psi_{1,2,1}^{(n)} \cos \tau + \Psi_{1,2,2}^{(n)} \cos 2\tau + \Psi_{1,2,3}^{(n)} \cos 3\tau \\ &\quad + \Psi_{1,2,4}^{(n)} \cos 4\tau + \Psi_{1,2,5}^{(n)} \cos 5\tau, \\ \bar{v}_{n2}(\tau) &= \Psi_{2,2,0}^{(n)} + \Psi_{2,2,1}^{(n)} \cos \tau + \Psi_{2,2,2}^{(n)} \cos 2\tau + \Psi_{2,2,3}^{(n)} \cos 3\tau \\ &\quad + \Psi_{2,2,4}^{(n)} \cos 4\tau + \Psi_{2,2,5}^{(n)} \cos 5\tau. \end{aligned} \tag{70}$$

Observing the solutions' structure at the first and the second iteration, the solutions at the k th iteration are written as follows:

$$\bar{u}_{nk}(\tau) = \sum_{j=0}^{2k+1} \Psi_{1,k,j}^{(n)} \cos(j\tau) \quad \text{and} \quad \bar{v}_{nk}(\tau) = \sum_{j=0}^{2k+1} \Psi_{2,k,j}^{(n)} \cos(j\tau), \tag{71}$$

where coefficients $\Psi_{i,k,j}^{(n)}$ are given as follows:

$$\Psi_{i,k,1}^{(n)} = C_{i,k,1}^{(n)} \quad \text{and} \quad \Psi_{i,k,j}^{(n)} = \frac{1}{(1-j^2)\omega^2} \Delta_{i,k,j}^{(n)}, \quad \text{for } j = 0, 2, 3, 4, \dots \tag{72}$$

So far, the procedure that may enable appropriate choices of the convergence-control parameters is yet to be presented. Once again, the squared residuals are used, and this time, they correspond to a higher-order deformation,

$$\begin{aligned}
 E_{m_1}(c_{0_1}, c_{0_2}) &= \frac{1}{2\pi} \int_0^{2\pi} \{\mathcal{A}_1[\tilde{u}_{n_m}(\tau)]\}^2 d\tau, \\
 E_{m_2}(c_{0_1}, c_{0_2}) &= \frac{1}{2\pi} \int_0^{2\pi} \{\mathcal{A}_2[\tilde{v}_{n_m}(\tau)]\}^2 d\tau.
 \end{aligned}
 \tag{73}$$

The convergence is guaranteed if the couple (c_{0_1}, c_{0_2}) minimizes at least one among the functions E_{m_1} and E_{m_2} and the norm of the vector (E_{m_1}, E_{m_2}) . However, in some cases where the expression of the squared residual is complex, making it difficult to find the minimum, the convergence control parameters are chosen by trial and error.

IV. NUMERICAL EXAMPLES

A. Example 1

In this first example, the results obtained with the HAM are compared to those calculated using the method described in Ref. 17, which is appropriate for simplified problems of forced transverse vibrations of double-beam systems. The studied double-beam system consists of two identical beams interconnected by an inner layer, and the whole system has the following characteristics: $L = 10$ m, $EI = 4 \times 10^6$ N m², $A = 5 \times 10^{-2}$ m², $\rho = 2 \times 10^3$ kg m⁻³, and $k_L = 2 \times 10^5$ N m⁻².

The natural frequencies corresponding to the first six modes are shown in Table I. A fair agreement is observed between the results obtained with the HAM at the fifth iteration and those obtained with the benchmark's method.

The transverse vibration of each beam is evaluated under two different simplified loading conditions: a concentrated harmonic load applied at the mid-span of the upper beam and a uniformly distributed harmonic load applied to the upper beam.

In Figs. 2 and 3, variations of dimensionless transverse displacements and curvatures with respect to dimensionless time are depicted. The amplitudes of the concentrated and uniformly distributed harmonic loads are 10 kN and 10 kN m⁻¹, respectively. Both excitations have a frequency of 100 rad/s. As with the natural frequencies, computations are performed up to the fifth iteration to

achieve convergence, and reasonable agreement between the HAM and Oniszczuk's method is observed. It can also be observed that the results of iteration 3 and iteration 4 differ significantly and that convergence occurs at iteration 4. The sudden change in the results from iteration 3 to iteration 4 demonstrates that the HAM algorithm's parameters and operators, specifically convergence control parameters, initial guesses, and linear operators, contribute to the convergence speed and algorithm's efficiency for the considered nonlinear mechanical system. A significant convergence speed is likely to lead to sudden changes in the results, as observed for iterations 3 and 4 in Figs. 2 and 3. The method proposed in Ref. 17 is a simplified approach only applicable to cases where axial forces, the mass per unit length of the inner layer, and its nonlinear stiffness coefficient are not considered. Nevertheless, the method remains reliable and can be adopted as a benchmark.

B. Example 2

In this example, the adopted double-beam system comprises two identical prismatic beams and an inner layer. A concentrated harmonic load of amplitude $P = 10$ kN is applied at the mid-span of the upper beam; the excitation has a frequency of 100 rad/s. The geometry and material characteristics are $L = 10$ m, $EI = 4 \times 10^6$ N m², $A = 5 \times 10^{-2}$ m², $\rho = 2 \times 10^3$ kg m⁻³, $k_L = 2 \times 10^5$ N m⁻², $\mu = 100$ kg m⁻¹, and $P_1 = P_2 = 10$ kN.

Regarding the initial conditions, instead of going from the initial configuration of the system given by $\tilde{w}_{i_0}(\xi)$ and the initial velocity field given by $\dot{\tilde{w}}_{i_0}(\xi)$ and employing the integrations of Eq. (15), the example is simplified by selecting the initial values of \tilde{u}_n and \tilde{v}_n and using Eq. (16) to calculate the initial values of \tilde{u}_{1_n} and \tilde{u}_{2_n} ; a value of -0.05×10^{-3} is adopted for both \tilde{u}_n and \tilde{v}_n . The value of -0.05×10^{-3} is in the order of magnitude of the dimensionless displacement values, as observed in the literature. The same values are adopted for the other numerical examples for the sake of simplification. Using Eq. (16), the initial values obtained for \tilde{u}_{1_n} and \tilde{u}_{2_n} are equal to -0.05×10^{-3} and 0, respectively.

The computed natural frequencies of the system for the first six modes and the first five iterations are presented in Table II. Unlike the lower frequencies $\omega_{k-1_2}^{(n)}$, the higher ones $\omega_{k-1_1}^{(n)}$ are not substantially influenced by the mode order. It also stands out that for both categories of frequencies, the finally adopted exact values

TABLE I. Comparison of the values of the natural frequency obtained with the HAM and Oniszczuk's method.

Mode (n=)	Natural frequency $\omega^{(n)}$ (rad/s)		Error (%)	Natural frequency $\omega^{(n)}$ (rad/s)		Error (%)
	Present study (Iter. 5)	Oniszczuk's method ¹⁷		Present study (Iter. 5)	Oniszczuk's method ¹⁷	
1	399.6	400.3	0.175	400.1	399.7	0.100
2	402.6	402.2	0.099	398.1	397.8	0.075
3	410.8	410.4	0.097	390.2	389.8	0.103
4	436.5	436.9	0.092	365.7	366.2	0.136
5	504.6	505.0	0.079	316.7	316.9	0.063
6	646.3	646.7	0.062	246.8	247.4	0.243

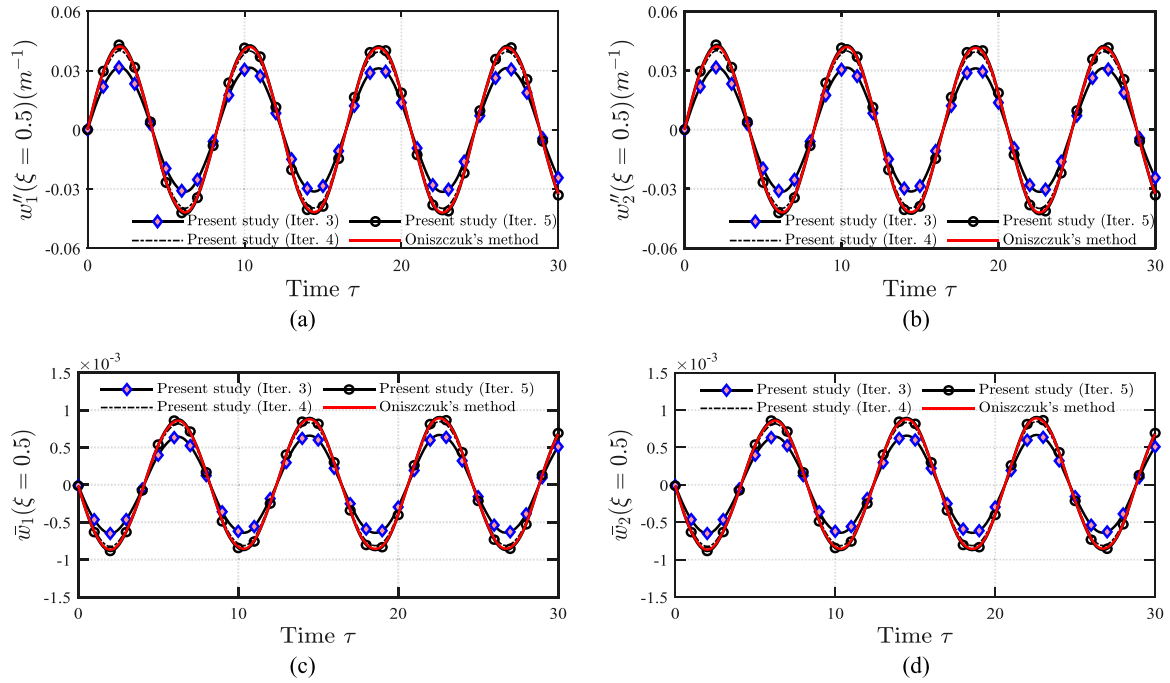


FIG. 2. Dimensionless displacements and curvatures in the case of a concentrated harmonic load applied to the upper beam. (a) Displacement at the mid-span of beam 1. (b) Curvature at the mid-span of beam 1. (c) Displacement at the mid-span of beam 2. (d) Curvature at the mid-span of beam 2.

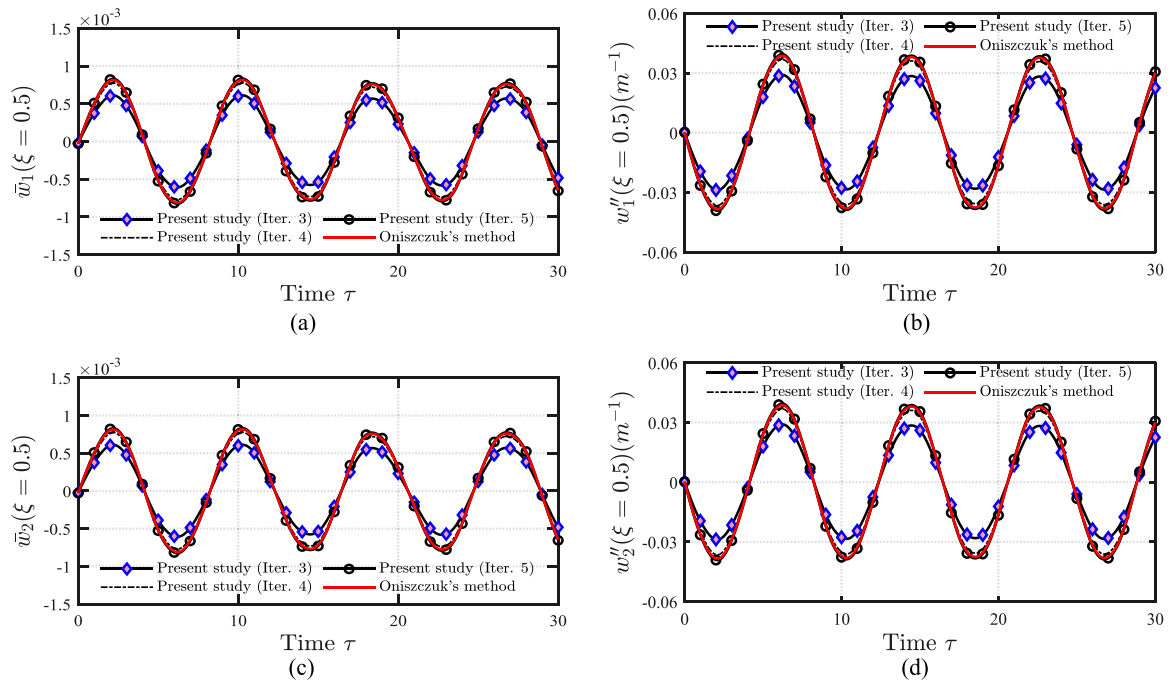


FIG. 3. Dimensionless displacements and curvatures at the mid-span of beam 1 and beam 2 in the case of a uniformly distributed harmonic load applied to the upper beam. (a) Displacement at the mid-span of beam 1. (b) Curvature at the mid-span of beam 1. (c) Displacement at the mid-span of beam 2. (d) Curvature at the mid-span of beam 2.

14 September 2023 13:11:11

TABLE II. Natural frequencies of a double-beam system made of two identical Euler–Bernoulli beams connected by an inner layer characterized by a linear stiffness coefficient $k_L = 2 \times 10^5 \text{ N m}^{-2}$ and a mass per unit length $\mu = 100 \text{ kg m}^{-1}$.

Mode (n=)	Natural frequency					Natural frequency				
	$\omega_{k-1_1}^{(n)}$ (rad/s) (kth iteration)					$\omega_{k-1_2}^{(n)}$ (rad/s) (kth iteration)				
	Iter. 1	Iter. 2	Iter. 3	Iter. 4	Iter. 5	Iter. 1	Iter. 2	Iter. 3	Iter. 4	Iter. 5
1	70.710	80.622	63.246	63.245	63.245	36.628	40.588	0.140	0.200	0.200
2	70.712	80.624	63.250	63.247	63.247	31.625	40.765	0.624	0.390	0.390
3	70.727	80.635	63.270	63.264	63.264	33.080	41.056	1.430	1.230	1.230
4	70.770	80.668	63.323	63.312	63.312	31.711	41.344	2.560	2.366	2.366
5	70.865	80.741	63.440	63.418	63.418	32.684	42.690	4.010	3.820	3.820
6	71.042	80.877	63.641	63.616	63.616	32.114	43.783	5.782	5.594	5.594

are obtained at the fourth iteration; however, the third iteration gives values very close to the adopted ones, demonstrating how fast convergence is achieved with the HAM.

In Figs. 4 and 5, the unknowns u_n and v_n , which are the solutions of Eq. (21), are shown as functions of the dimensionless time. The dependence of these functions on the mode shape function is weak, which explains why the curves corresponding to all modes have a nearly identical trend. The same explanation applies to the time-dependent parts of the dynamic responses depicted in Figs. 6

and 7, deduced from Eq. (16). The most important observation from these figures is how fast the convergence is reached.

The double-beam system under consideration is subjected to a fixed concentrated harmonic load with an amplitude of $P = 10 \text{ kN}$, acting at the mid-span of the upper beam. In this case, the nonlinear stiffness coefficient k_{NL} of the inner layer is not considered. Due to this assumption, the convergence is reached very fast when calculating the modal natural frequencies given in Table II. Regarding the system’s dynamic response, namely, the transverse vibrations of each

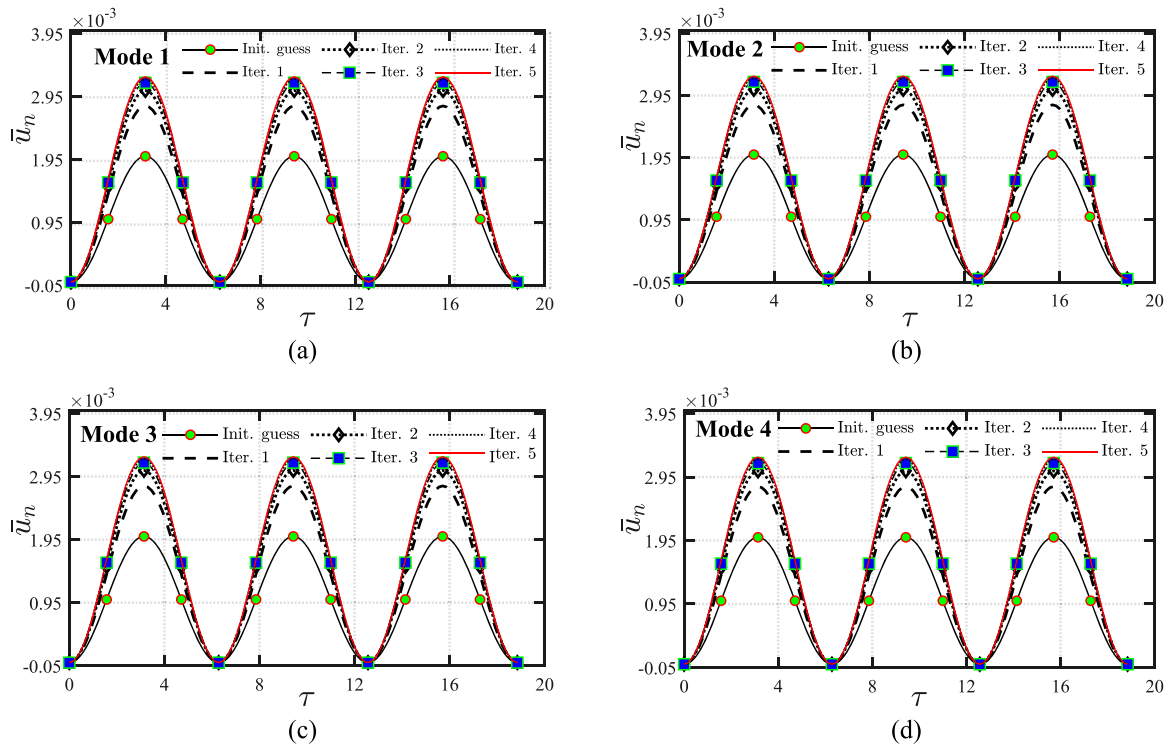


FIG. 4. Variation in the time-dependent unknown function u_n for the first four modes and the first five iterations from the initial guess u_0 : $k_L = 2 \times 10^5 \text{ N m}^{-2}$, $\mu = 0$, and $k_{NL} = 0$. (a) First mode ($n = 1$); (b) second mode ($n = 2$); (c) third mode ($n = 3$); (d) fourth mode ($n = 4$).

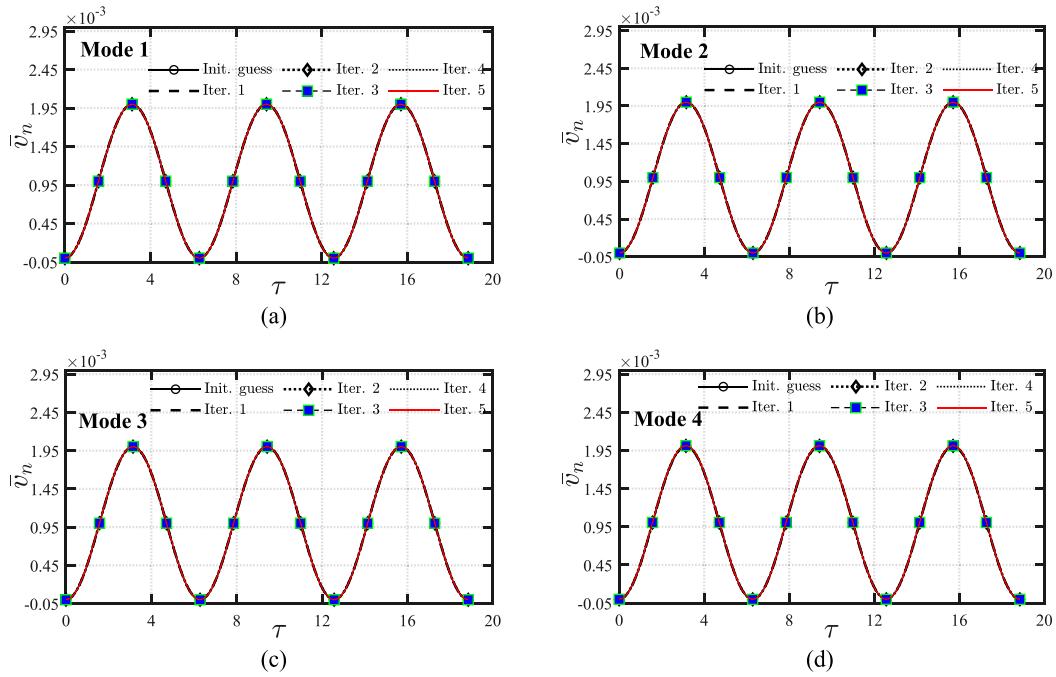


FIG. 5. Variation in the time-dependent unknown function v_n for the first four modes and the first five iterations from the initial guess v_0 : $k_L = 2 \times 10^5 \text{ N m}^{-2}$, $\mu = 0$, and $k_{NL} = 0$. (a) First mode ($n = 1$); (b) second mode ($n = 2$); (c) third mode ($n = 3$); (d) fourth mode ($n = 4$).

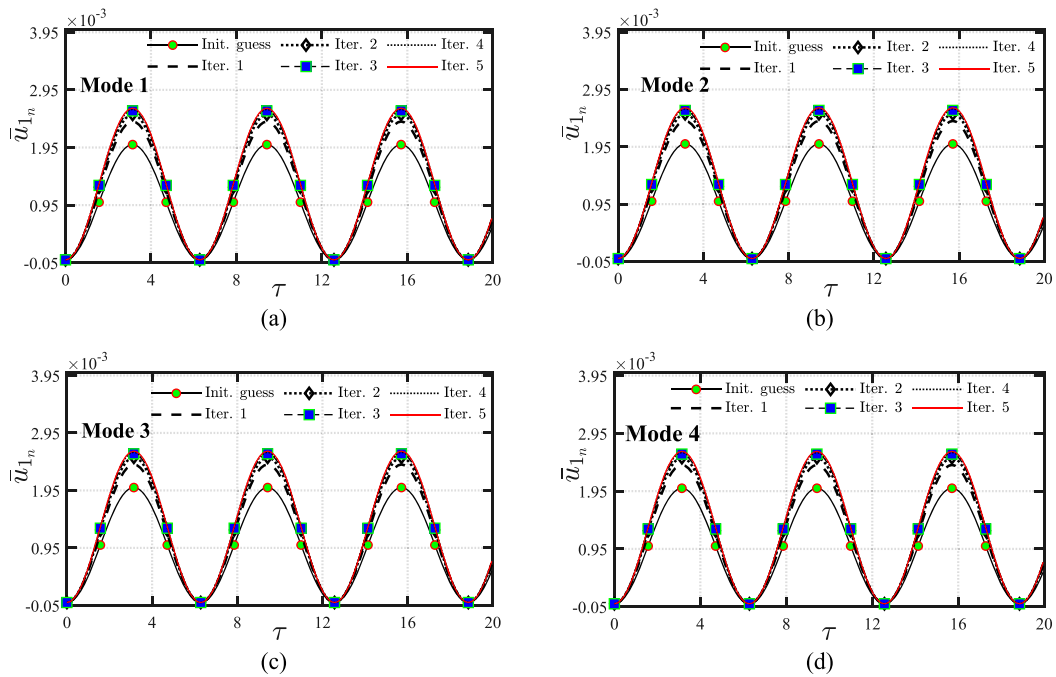


FIG. 6. Temporal variation in u_{1n} , representing the dimensionless time-dependent part of the transverse displacement of beam 1 for the first four modes and the first five iterations: $k_L = 2 \times 10^5 \text{ N m}^{-2}$, $\mu = 0$, and $k_{NL} = 0$. (a) First mode ($n = 1$); (b) second mode ($n = 2$); (c) third mode ($n = 3$); (d) fourth mode ($n = 4$).

14 September 2023 13:11:11

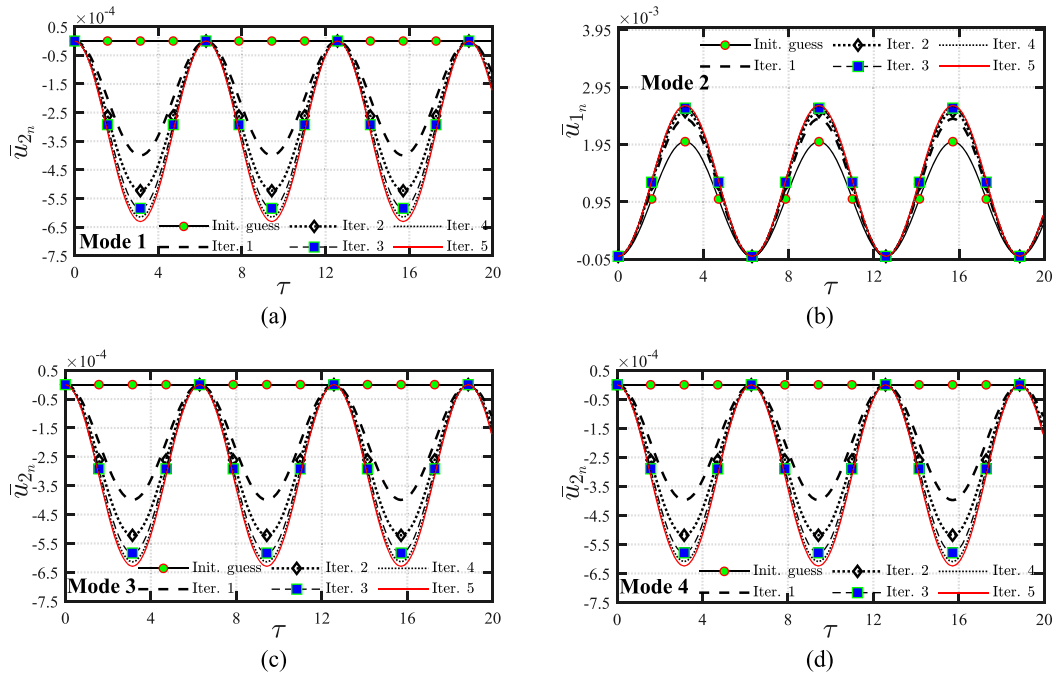


FIG. 7. Temporal variation in u_{2n} representing the dimensionless time-dependent part of the transverse displacement of beam 1 for the first four modes and the first five iterations: $k_L = 2 \times 10^5 \text{ N m}^{-2}$, $\mu = 0$, and $k_{NL} = 0$. (a) First mode ($n = 1$); (b) second mode ($n = 2$); (c) third mode ($n = 3$); (d) fourth mode ($n = 4$).

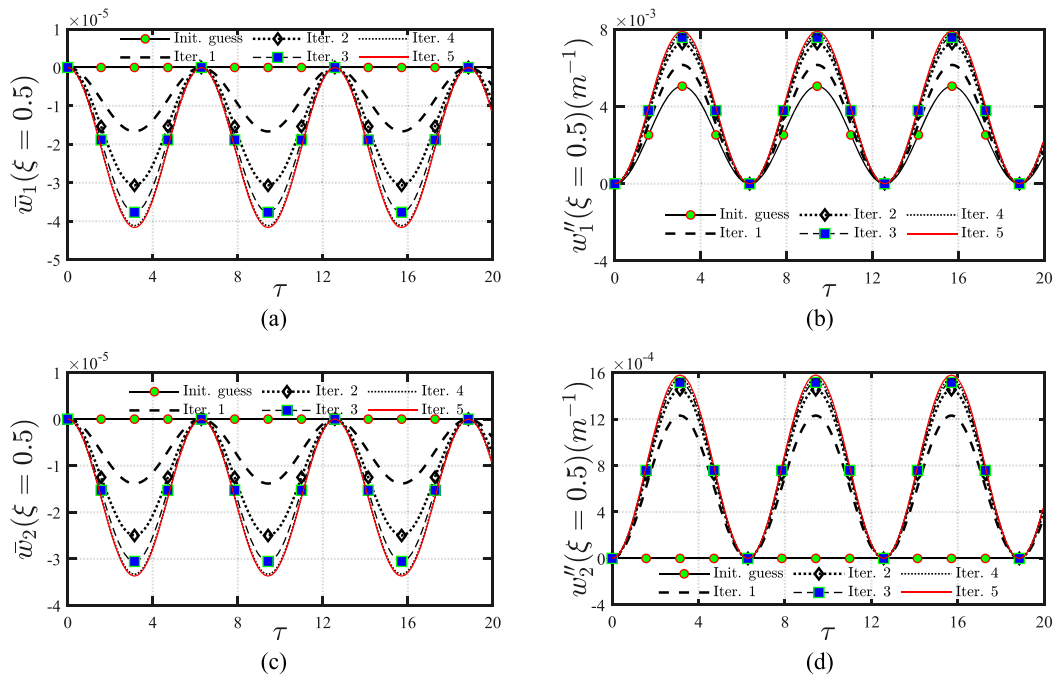


FIG. 8. Dimensionless displacements and curvatures at the mid-span of beam 1 and beam 2 for the first five homotopy iterations obtained from the superposition of the first eight modes: $k_L = 2 \times 10^5 \text{ N m}^{-2}$, $\mu = 0$, and $k_{NL} = 0$. (a) Displacement at the mid-span of beam 1; (b) curvature at the mid-span of beam 1; (c) displacement at the mid-span of beam 2; (d) curvature at the mid-span of beam 2.

14 September 2023 13:11:11

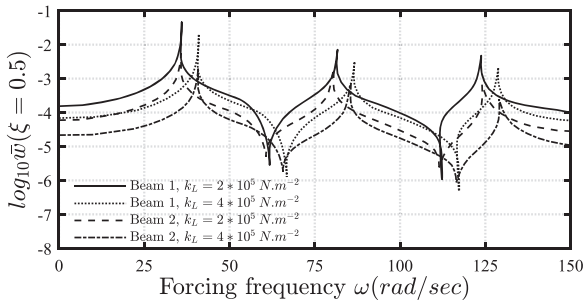


FIG. 9. Effects of parameter k_L on the frequency response at the mid-span of beam 1 and beam 2.

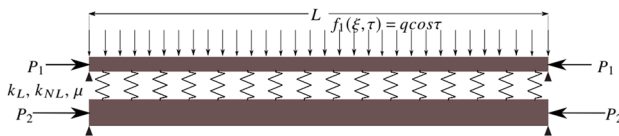


FIG. 10. Two-dimensional model of a double-beam system subjected to axial loads and a uniformly distributed harmonic load applied to the upper beam.

beam, they can now be obtained from the computed time-dependent unknowns. The modal superposition principle is used for this purpose. In Fig. 8 temporal variations of the non-dimensionalized transverse vibrations and curvatures of each beam at the mid-span

are presented. These graphs are constructed by superposing the results of the first eight modes. The analysis of the system’s frequency response at the mid-span for the forcing frequency range of 0–150 rad/s is depicted in Fig. 9; the figure reveals that, for the six observed modes, resonance happens at the first one. Furthermore, it can be seen that the linear stiffness coefficient slightly affects the vibration amplitude.

C. Example 3

In the following example, the considered double-beam system depicted in Fig. 10 comprises two non-identical beams. The upper beam is acted upon by a uniformly distributed harmonic load with the amplitude $q = 10 \text{ kN m}^{-1}$ and a frequency equal to 100 rad/s. The two beams are axially loaded by the compressive axial loads $P_1 = P_2 = 10 \text{ kN}$. The other parameters are given as follows: length $L_1 = L_2 = 10 \text{ m}$, flexural stiffness $E_1 I_1 = 10^7 \text{ N m}^2$ and $E_2 I_2 = 1.5 \times 10^9 \text{ N m}^2$, mass per unit length of beams $\rho_1 A_1 = 100 \text{ kg m}^{-1}$ and $\rho_2 A_2 = 3500 \text{ kg m}^{-1}$, linear stiffness coefficient of the inner layer $k_L = 4 \times 10^7 \text{ N m}^{-2}$, nonlinear stiffness coefficient of the inner layer $k_{NL} = 10^{13} \text{ N m}^{-4}$, and mass per unit length of the inner layer $\mu = 100 \text{ kg m}^{-1}$.

Various computations are performed to gain insight into the effect of the nonlinear stiffness coefficient and the inner layer’s mass per unit length. In the first case where these two parameters are ignored in the algorithm, variations in the dimensionless transversal displacements and curvatures, constructed from the superposition of the first eight modal results, are shown in Fig. 11. Furthermore,

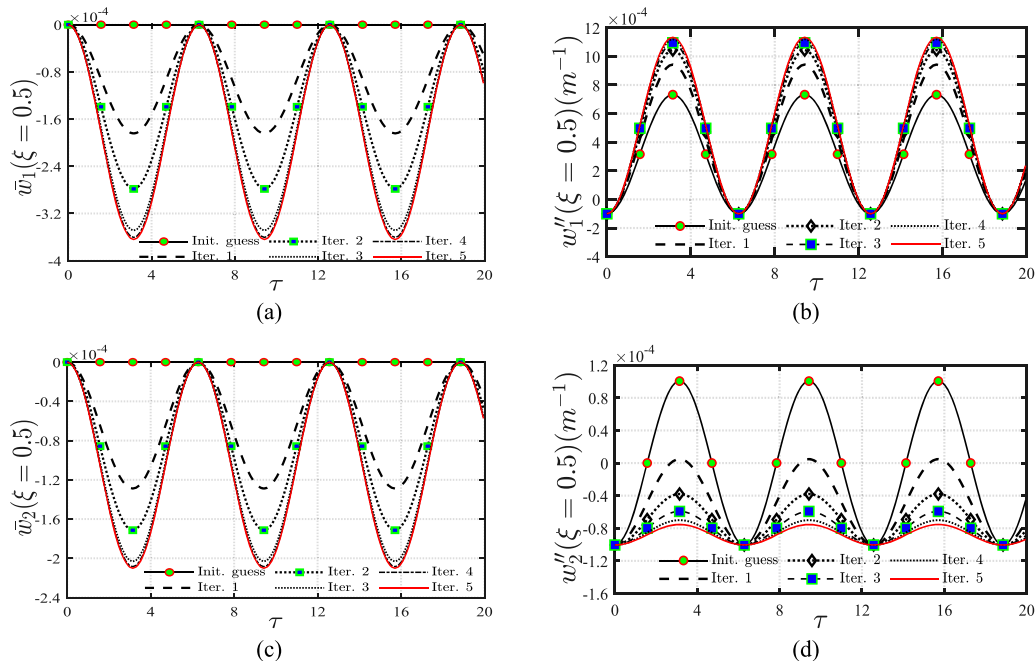


FIG. 11. Dimensionless displacements and curvatures at the mid-span of beam 1 and beam 2 for the first five homotopy iterations obtained from the superposition of the first eight modes: $k_L = 4 \times 10^7 \text{ N m}^{-2}$, $\mu = 0$, and $k_{NL} = 0$. (a) Displacement at the mid-span of beam 1; (b) curvature at the mid-span of beam 1; (c) displacement at the mid-span of beam 2; (d) curvature at the mid-span of beam 2.

14 September 2023 13:11:11

TABLE III. Natural frequencies: $k_L = 4 \times 10^7 \text{ N m}^{-2}$, $\mu = 0$, and $k_{NL} = 0$.

Mode (n=)	Natural frequency					Natural frequency				
	$\omega_{k-1_1}^{(n)}$ (rad/s) (kth iteration)					$\omega_{k-1_2}^{(n)}$ (rad/s) (kth iteration)				
	Iter. 1	Iter. 2	Iter. 3	Iter. 4	Iter. 5	Iter. 1	Iter. 2	Iter. 3	Iter. 4	Iter. 5
1	580.830	581.690	579.968	579.968	579.968	88.219	108.572	86.550	86.550	86.550
2	580.831	581.700	579.970	579.970	579.970	121.194	149.178	118.950	118.951	118.951
3	580.838	581.703	579.975	579.975	579.975	155.891	191.770	152.764	152.763	152.763
4	580.841	581.706	579.980	579.980	579.980	168.408	207.498	165.707	165.707	165.707
5	580.884	581.750	580.013	580.013	580.013	205.265	252.060	200.254	200.254	200.254
6	580.900	581.762	580.020	580.020	580.020	203.145	250.953	201.240	201.239	201.239

TABLE IV. Natural frequencies: $k_L = 4 \times 10^7 \text{ N m}^{-2}$, $\mu = 100 \text{ kg m}^{-1}$, and $k_{NL} = 0$.

Mode (n=)	Natural frequency					Natural frequency				
	$\omega_{k-1_1}^{(n)}$ (rad/s) (kth iteration)					$\omega_{k-1_2}^{(n)}$ (rad/s) (kth iteration)				
	Iter. 1	Iter. 2	Iter. 3	Iter. 4	Iter. 5	Iter. 1	Iter. 2	Iter. 3	Iter. 4	Iter. 5
1	660.587	771.910	579.981	579.981	579.981	78.681	93.688	67.476	67.476	67.476
2	660.514	771.791	579.970	579.970	579.970	108.091	128.730	92.747	92.747	92.747
3	660.802	772.250	580.308	580.308	580.308	139.037	165.476	119.058	119.058	119.058
4	660.075	771.059	579.172	579.172	579.172	150.201	179.064	129.307	129.307	129.307
5	661.626	773.540	581.552	581.552	581.552	183.072	217.490	155.884	155.884	155.884
6	658.906	769.091	577.328	577.328	577.328	181.182	216.605	157.382	157.382	157.382

this figure gives insights into how fast the convergence is achieved. The observed displacements are consistent with the beams' characteristics. Indeed, the lower beam, being stiffer than the upper, undergoes smaller displacements than the upper one. A more reliable assessment of the convergence is possible by observing the natural frequencies given in Tables III and IV. In Table III, the natural frequencies are computed with k_{NL} and μ not accounted for, and those given in Table IV are computed with $\mu = 100 \text{ kg m}^{-1}$. In both cases, the exact values of the natural frequency are obtained at the third iteration.

The results of the frequency response analysis are presented in Fig. 12 for the first case where parameters k_{NL} and μ are disregarded and in Fig. 13 for the second case where these parameters are accounted for. For the first case, resonance happens at the first mode, and for the second case, resonance happens at the first and second modes. It should be noted again that these observations are limited to the number of computed modal results.

Two different trends are observed for the natural frequencies $\omega_{k-1_1}^{(n)}$ and $\omega_{k-1_2}^{(n)}$:

- the natural frequencies $\omega_{k-1_1}^{(n)}$ are not much affected by the change in the value of μ . Observing the exact values in Tables III and IV, at the fifth iteration, for instance, the values are slightly increased for the odd order modes and slightly decreased for the even order modes;

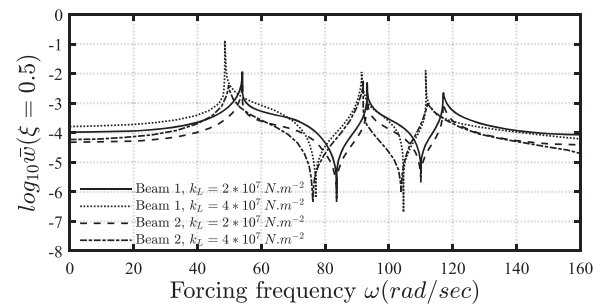


FIG. 12. Effects of the parameter k_L on the frequency response at the mid-span of beam 1 and beam 2.

- regarding the natural frequencies $\omega_{k-1_2}^{(n)}$, a significant decrease is observed when the mass of the inner layer changes from 0 to 100 kg m^{-1} .

Further calculations of the natural frequency are performed for several values of the stiffness coefficient; the results of the first case where μ and k_{NL} are ignored are shown in Fig. 14. Similar calculations are performed for the remaining three cases (at least one of the parameters μ and k_{NL} is not ignored) (see Figs. 15–17) in order to

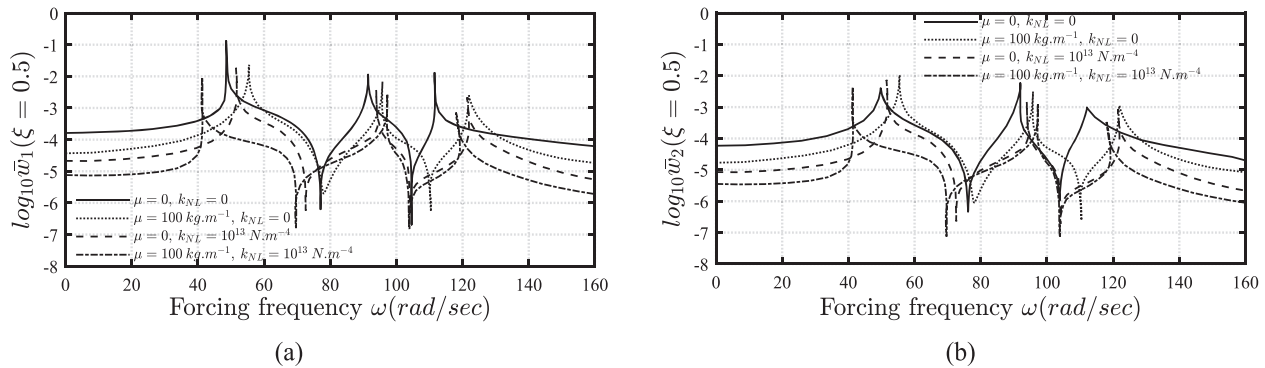


FIG. 13. Effects of the parameters μ and k_{NL} on the frequency response at the mid-span of beam 1 and beam 2. (a) Frequency response at the mid-span of beam 1; (b) frequency response at the mid-span of beam 2.

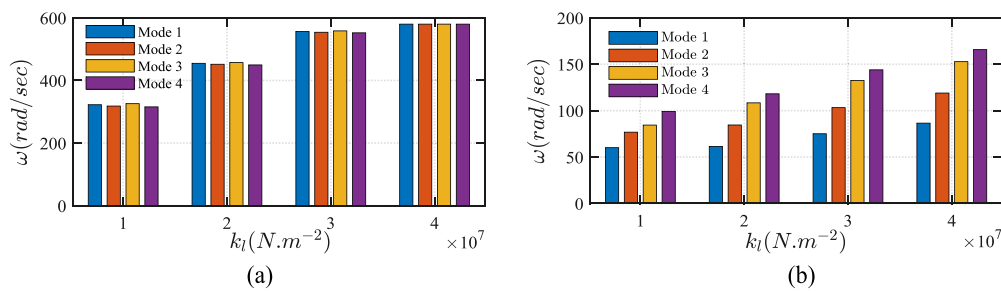


FIG. 14. Frequencies $\omega_{4_1}^{(n)}$ and $\omega_{4_2}^{(n)}$ for different values of the stiffness coefficient: $\mu = 0$ and $k_{NL} = 0$. (a) Frequency $\omega_{4_1}^{(n)}$ (5th iteration); (b) frequency $\omega_{4_2}^{(n)}$ (5th iteration).

highlight the simultaneous influence of at least two of the parameters k_L , k_{NL} , and μ .

When the parameter k_{NL} is accounted for in the calculation, there is an increase in the number of iterations needed to achieve convergence. For the previous cases, the exact values of the natural frequencies are obtained at the third iteration even though calculations are performed up to the fifth iteration, and five iterations are needed to obtain the exact trends of the graphs representing dimensionless displacements and curvatures. When $k_{NL} = 10^{13} \text{ N m}^{-4}$, computations need to be performed up to six iterations to reach

the convergence, as it can be observed in Tables V and VI. With the same value of k_{NL} , two different cases are considered for $\mu = 0$ and $\mu = 100 \text{ kg m}^{-1}$, corresponding to natural frequencies given in Tables V and VI, respectively. Unlike the previous observation made about the effect of the parameter μ , when k_{NL} was not accounted for, taking into account k_{NL} reduces significantly the influence of μ . This results from the fact that the nonlinear stiffness coefficient is a very big number compared to the mass per unit length.

Dimensionless transverse displacements and curvatures are plotted using $k_{NL} = 10^{13} \text{ N m}^{-4}$ and $\mu = 100 \text{ kg m}^{-1}$. Prior to this,

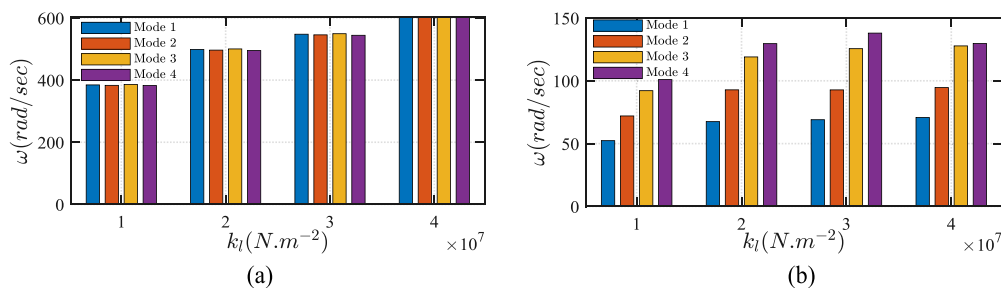


FIG. 15. Frequencies $\omega_{4_1}^{(n)}$ and $\omega_{4_2}^{(n)}$ for different values of the stiffness coefficient: $\mu = 100 \text{ kg m}^{-1}$ and $k_{NL} = 0$. (a) Frequency $\omega_{4_1}^{(n)}$ (5th iteration); (b) frequency $\omega_{4_2}^{(n)}$ (5th iteration).

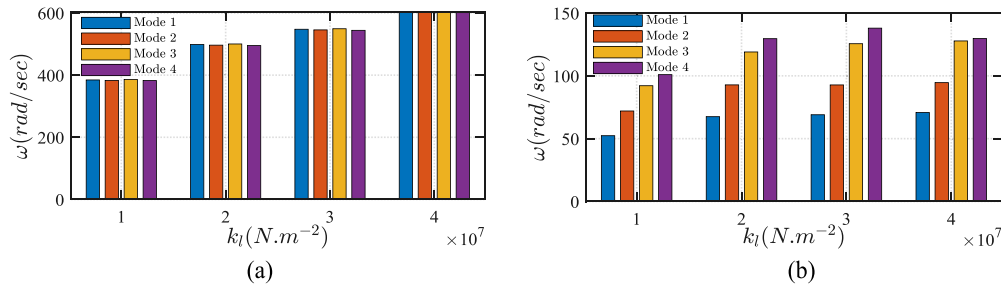


FIG. 16. Frequencies $\omega_{S_1}^{(n)}$ and $\omega_{S_2}^{(n)}$ for different values of the stiffness coefficient: $\mu = 0$ and $k_{NL} = 10^{13} \text{ N m}^{-4}$. (a) Frequency $\omega_{S_1}^{(n)}$ (6th iteration); (b) frequency $\omega_{S_2}^{(n)}$ (6th iteration).

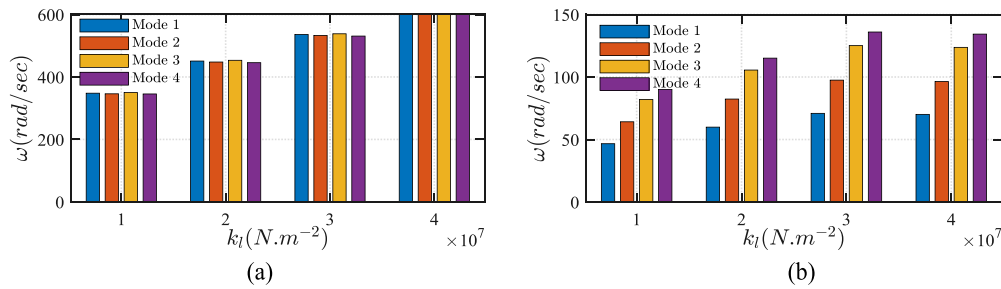


FIG. 17. Frequencies $\omega_{S_1}^{(n)}$ and $\omega_{S_2}^{(n)}$ for different values of the stiffness coefficient: $\mu = 100 \text{ kg m}^{-1}$ and $k_{NL} = 10^{13} \text{ N m}^{-4}$. (a) Frequency $\omega_{S_1}^{(n)}$ (6th iteration); (b) frequency $\omega_{S_2}^{(n)}$ (6th iteration).

the time-dependent unknown functions u_n and v_n are computed and plotted in Figs. 18 and 19, and time-dependent parts of dimensionless displacements u_{1n} and u_{2n} are deduced and plotted in Figs. 20 and 21. It appears again that the functions u_n , v_n , u_{1n} , and u_{2n} are not significantly affected by the mode order; the reason lies in the weak dependence on mode shape functions of the coefficients of the solved system of ODEs. The superposition of the first eight modal results gives the total displacement whose temporal variation at the mid-span and the corresponding curvature are plotted in Fig. 22.

The influence of the parameters k_{NL} and μ is noticeable when comparing the results of deflections and curvatures in Figs. 11 and 22. In Fig. 11, the two beams appear to behave differently, with marked discrepancies in the results. A different picture is provided in the results depicted in Fig. 22, where the incorporation of k_{NL} and μ leads to greater synergy in the double-beam system and the same behavior of the two beams.

The influence of the nonlinear stiffness coefficient is highlighted by comparing Figs. 11 and 22. Besides the difference in the

TABLE V. Natural frequencies: $k_L = 4 \times 10^7 \text{ N m}^{-2}$, $\mu = 0$, and $k_{NL} = 10^{13} \text{ N m}^{-4}$.

Mode (n=)	Natural frequency						Natural frequency					
	$\omega_{k-1_1}^{(n)}$ (rad/s) (kth iteration)						$\omega_{k-1_2}^{(n)}$ (rad/s) (kth iteration)					
	Iter. 1	Iter. 2	Iter. 3	Iter. 4	Iter. 5	Iter. 6	Iter. 1	Iter. 2	Iter. 3	Iter. 4	Iter. 5	Iter. 6
1	662.374	778.585	594.322	597.683	602.007	602.008	79.760	95.512	69.924	70.316	70.820	70.820
2	662.300	778.466	594.210	597.573	601.900	601.900	106.477	127.527	93.395	93.918	94.589	94.589
3	662.576	778.910	594.614	597.971	602.300	602.303	144.113	172.490	126.160	126.870	127.783	127.783
4	661.824	777.706	593.490	596.863	601.200	601.200	145.530	174.477	128.083	128.791	129.668	129.670
5	663.312	780.104	595.670	599.008	603.306	603.305	194.657	232.550	169.512	170.480	171.729	171.730
6	660.492	775.604	591.497	594.892	599.260	599.260	173.001	207.953	153.673	154.497	155.541	155.542

TABLE VI. Natural frequencies: $k_L = 4 \times 10^7 \text{ N m}^{-2}$, $\mu = 100 \text{ kg m}^{-1}$, and $k_{NL} = 10^{13} \text{ N m}^{-4}$.

Mode (n=)	Natural frequency						Natural frequency					
	$\omega_{k-1}^{(n)}$ (rad/s) (kth iteration)						$\omega_{k-2}^{(n)}$ (rad/s) (kth iteration)					
	Iter. 1	Iter. 2	Iter. 3	Iter. 4	Iter. 5	Iter. 6	Iter. 1	Iter. 2	Iter. 3	Iter. 4	Iter. 5	Iter. 6
1	662.374	778.585	594.322	597.683	602.007	602.008	78.957	94.551	69.220	69.608	70.106	70.105
2	662.302	778.468	594.214	597.577	601.903	601.904	108.470	129.914	95.143	95.675	96.360	96.360
3	662.590	778.923	594.634	597.990	602.309	602.309	139.526	167.001	122.140	122.827	123.711	123.711
4	661.864	777.745	593.551	596.924	601.261	601.260	150.727	180.710	132.637	133.372	134.314	134.314
5	663.411	780.198	595.820	599.160	603.460	603.459	183.720	219.500	159.936	160.852	162.036	162.037
6	660.700	775.800	591.796	595.194	599.563	599.563	181.813	218.586	161.404	162.274	163.381	163.380

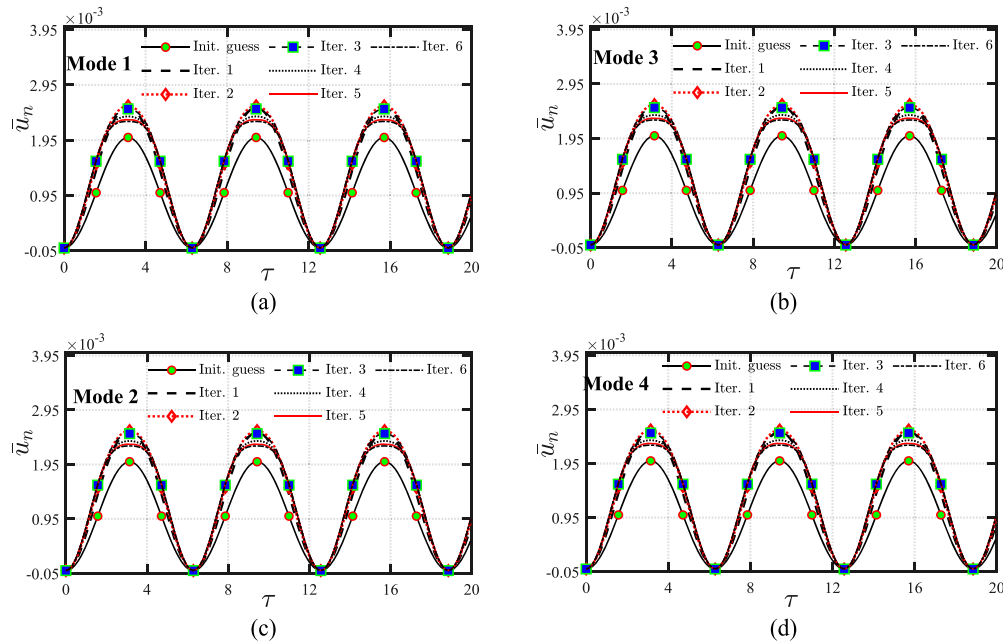


FIG. 18. Variation in the time-dependent unknown function u_n for the first four modes and the first six iterations from the initial guess u_0 : $k_L = 4 \times 10^7 \text{ N m}^{-2}$, $\mu = 100 \text{ kg m}^{-1}$, and $k_{NL} = 10^{13} \text{ N m}^{-4}$. (a) First mode ($n = 1$); (b) second mode ($n = 2$); (c) third mode ($n = 3$); (d) fourth mode ($n = 4$).

number of iterations required to achieve the convergence, there is a notable difference in the pace of the plotted curves.

With the time-dependent parts of the dynamic response at each mode being known, three-dimensional surfaces representing variations in the displacement with time and position can be constructed. For the sake of clarity, each of the first four modal dimensionless displacements is presented in Fig. 23 for the upper beam and in Fig. 24 for the lower beam.

D. Example 4

We consider the double-beam system given in the preceding example, subjected to a constant moving load of magnitude $g_1 = 160 \text{ kN}$ applied to the upper beam. Computations are con-

ducted for moving speeds of 40 and 100 m s^{-1} . We consider 4 different combinations of k_{NL} and μ .

The results obtained from the sixth homotopy iteration and the superposition of the first eight modal responses are depicted in Fig. 25, where graphs of the variations of the dimensionless displacement at the mid-span of each beam vs the dimensionless time are plotted. The influence of the inner layer characteristics and the load speed is observed. One direct observation concerns the occurrence of the maximum deflection. It is noticed that the maximum deflection of the lower beam occurs for almost the same value of the dimensionless time. If parameter k_{NL} is equal to 0, values of the maximum deflections of the two beams are not substantially affected by the increase in the mass per unit length of the inner layer.

14 September 2023 13:11:11

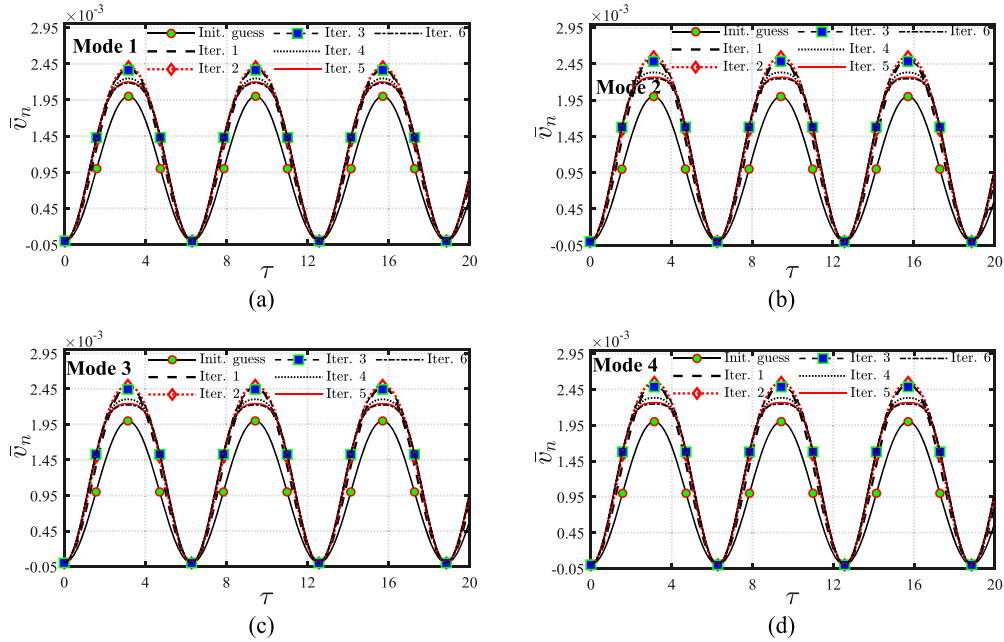


FIG. 19. Variation in the time-dependent unknown function v_n for the first four modes and the first six iterations from the initial guess v_0 : $k_L = 4 \times 10^7 \text{ N m}^{-2}$, $\mu = 100 \text{ kg m}^{-1}$, and $k_{NL} = 10^{13} \text{ N m}^{-4}$. (a) First mode ($n = 1$); (b) second mode ($n = 2$); (c) third mode ($n = 3$); (d) fourth mode ($n = 4$).

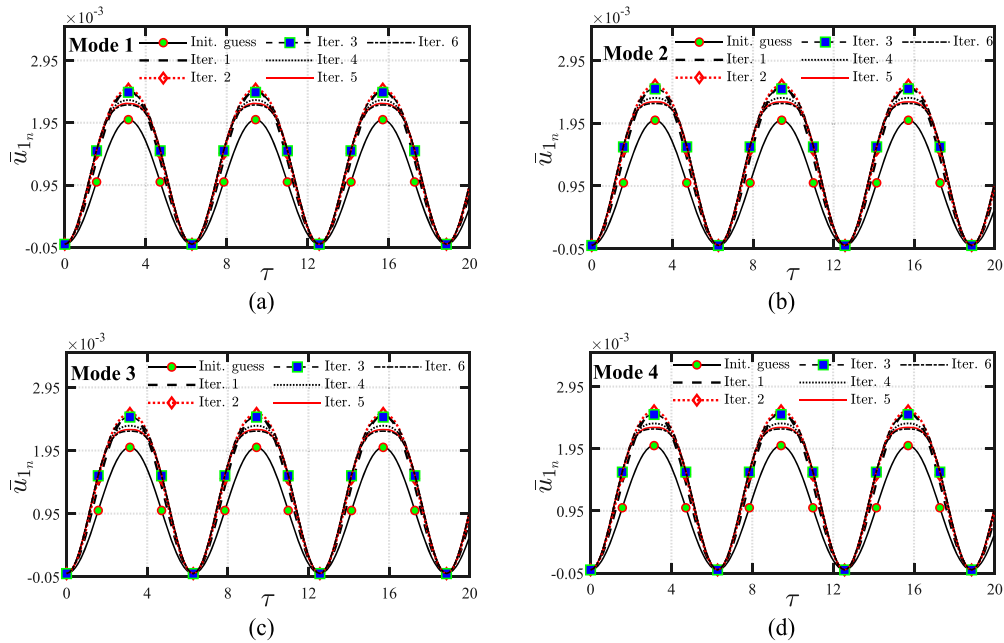


FIG. 20. Temporal variation in u_{1n} , representing the time-dependent part of the transverse displacement of beam 1 for the first four modes and the first six iterations: $k_L = 4 \times 10^7 \text{ N m}^{-2}$, $\mu = 100 \text{ kg m}^{-1}$, and $k_{NL} = 10^{13} \text{ N m}^{-4}$. (a) First mode ($n = 1$); (b) second mode ($n = 2$); (c) third mode ($n = 3$); (d) fourth mode ($n = 4$).

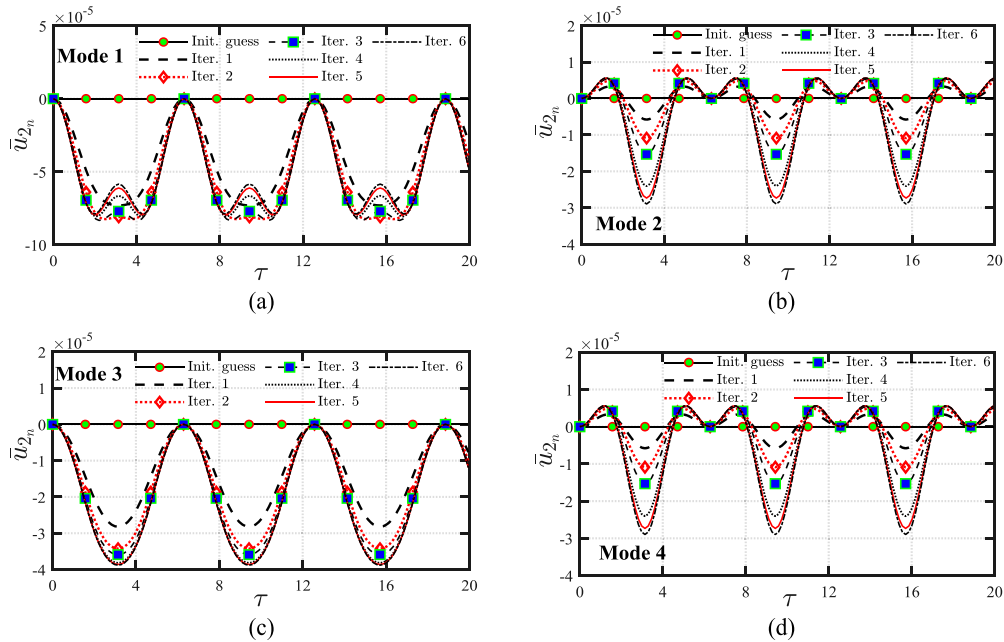


FIG. 21. Temporal variation in u_{2n} representing the time-dependent part of the transverse displacement of beam 2 for the first four modes and the first six iterations: $k_L = 4 \times 10^7 \text{ N m}^{-2}$, $\mu = 100 \text{ kg m}^{-1}$, and $k_{NL} = 10^{13} \text{ N m}^{-4}$. (a) First mode ($n = 1$); (b) second mode ($n = 2$); (c) third mode ($n = 3$); (d) fourth mode ($n = 4$).

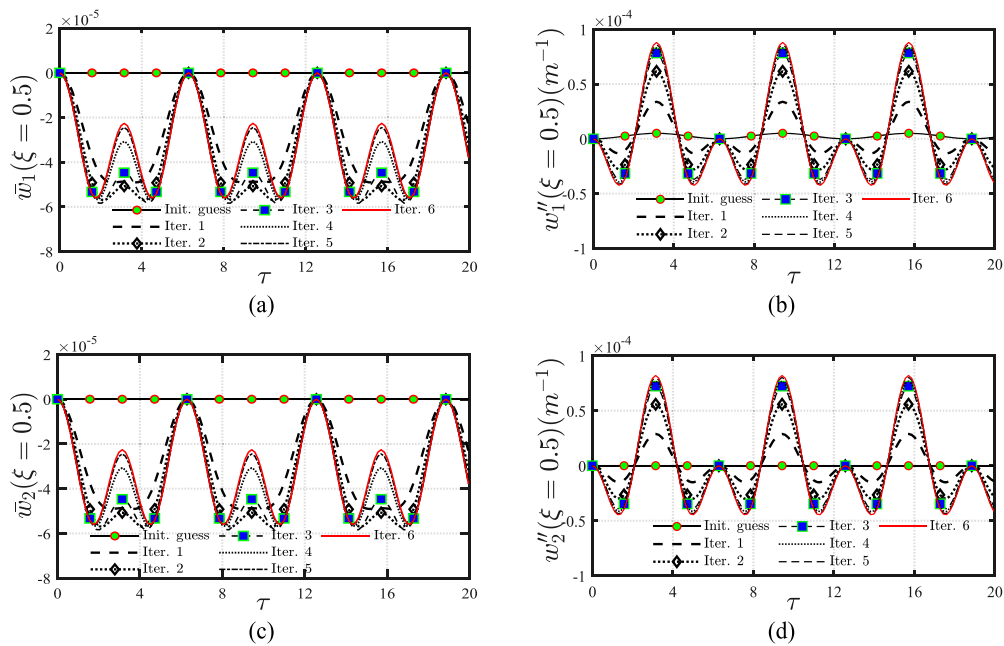


FIG. 22. Dimensionless displacements at the mid-span of beam 1 and beam 2 for the first six homotopy iterations obtained from the superposition of the first eight modes: $k_L = 4 \times 10^7 \text{ N m}^{-2}$, $\mu = 100 \text{ kg m}^{-1}$, and $k_{NL} = 10^{13} \text{ N m}^{-4}$. (a) Displacement at the mid-span of beam 1; (b) curvature at the mid-span of beam 1; (c) displacement at the mid-span of beam 2; (d) curvature at the mid-span of beam 2.

14 September 2023 13:11:11

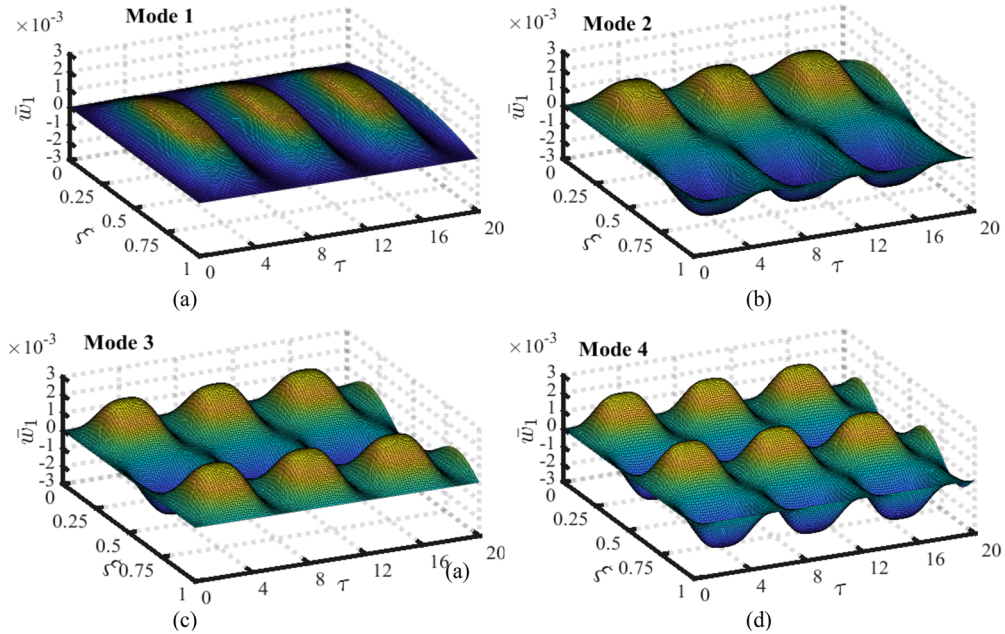


FIG. 23. Variations in dimensionless displacements of the upper beam with dimensionless time and position for the first four modes: $k_L = 4 \times 10^7 \text{ N m}^{-2}$, $\mu = 100 \text{ kg m}^{-1}$, and $k_{NL} = 10^{13} \text{ N m}^{-4}$. (a) First mode ($n = 1$); (b) second mode ($n = 2$); (c) third mode ($n = 3$); (d) fourth mode ($n = 4$).

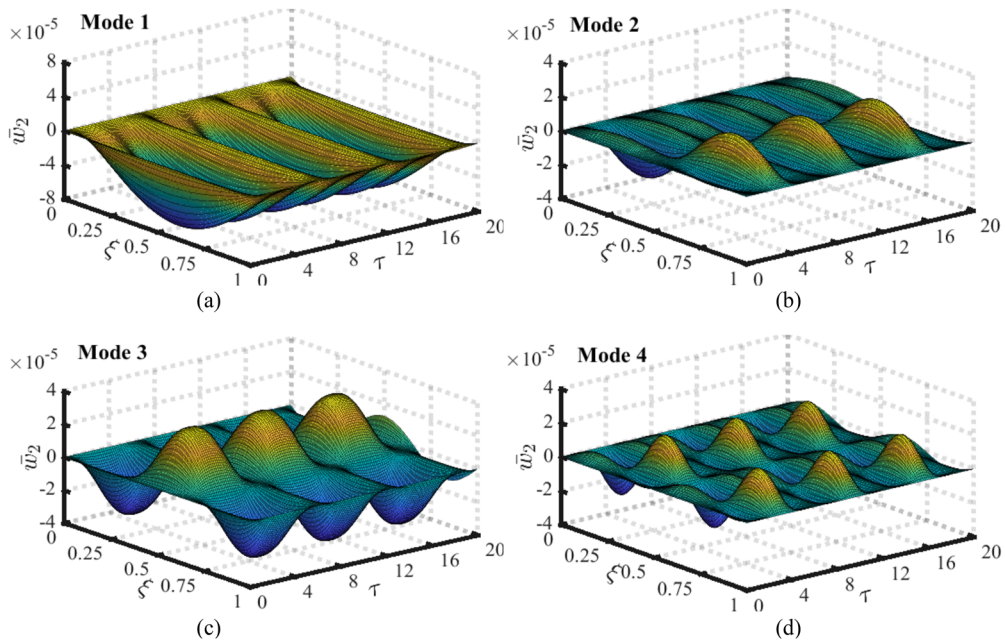


FIG. 24. Variations in dimensionless displacements of the lower beam with dimensionless time and position for the first four modes: $k_L = 4 \times 10^7 \text{ N m}^{-2}$, $\mu = 100 \text{ kg m}^{-1}$, and $k_{NL} = 10^{13} \text{ N m}^{-4}$. (a) First mode ($n = 1$); (b) second mode ($n = 2$); (c) third mode ($n = 3$); (d) fourth mode ($n = 4$).

14 September 2023 13:11:11

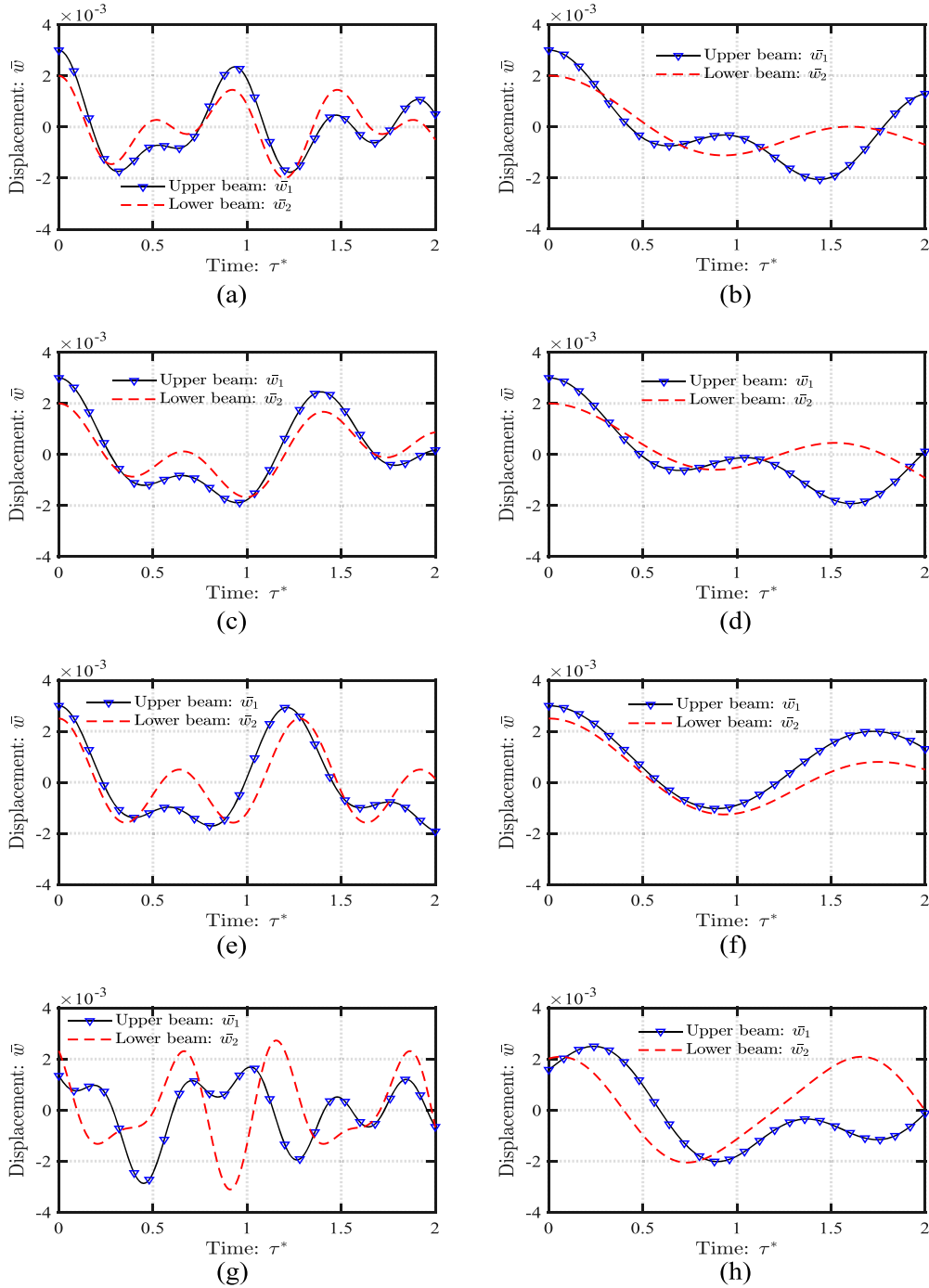


FIG. 25. Dimensionless displacements at the mid-span of beam 1 and beam 2 from the sixth homotopy iteration, under a constant moving load of magnitude 160 kN applied to the upper beam: $k_L = 4 \times 10^7 \text{ N m}^{-2}$. (a) $v = 40 \text{ m s}^{-1}$, $k_{NL} = 0$, and $\mu = 0$; (b) $v = 100 \text{ m s}^{-1}$, $k_{NL} = 0$, and $\mu = 0$; (c) $v = 40 \text{ m s}^{-1}$, $k_{NL} = 0$, and $\mu = 100 \text{ kg m}^{-1}$; (d) $v = 100 \text{ m s}^{-1}$, $k_{NL} = 0$, and $\mu = 100 \text{ kg/m}$; (e) $v = 40 \text{ m s}^{-1}$, $k_{NL} = 10^{13}$, and $\mu = 0$; (f) $v = 100 \text{ m s}^{-1}$, $k_{NL} = 10^{13}$, and $\mu = 0$; (g) $v = 40 \text{ m s}^{-1}$, $k_{NL} = 10^{13}$, and $\mu = 100 \text{ kg m}^{-1}$; (h) $v = 100 \text{ m s}^{-1}$, $k_{NL} = 10^{13}$, and $\mu = 100 \text{ kg m}^{-1}$.

14 September 2023 13:11:11

V. CONCLUSION

This paper presented the HAM for analyzing transverse vibrations of axially and transversally loaded simply supported double-beam systems comprising two prismatic parallel Euler–Bernoulli beams of equal length, interconnected by an inner layer characterized by linear and nonlinear stiffness coefficients. The system's motion is described by a set of nonlinear PDEs derived from the Euler–Bernoulli theory. At the beginning of the procedure, the mode shape function consistent with the chosen boundary conditions enabled, through the Bubnov–Galerkin method, removal of the spatial variable and transformed the system of PDEs into a system of ODEs that was solved with the HAM. The solutions of the system of ODEs are time-dependent functions involved in the modal superposition technique to construct the dynamic response of the system.

Natural frequencies corresponding to the n -th mode at the k -th iteration were easily computed by setting the coefficients of the terms in the k -th order deformation equations that are likely to generate the so-called secular terms in the solution to zero. In addition, the effects of the nonlinear stiffness coefficient and the mass per unit length of the inner layer were explored. It was observed that the incorporation of the nonlinear stiffness coefficient substantially affected the dynamic response and natural frequencies. Moreover, a subtle difference in the natural frequencies was observed when accounting for the mass per unit length.

The efficiency of the algorithm has been demonstrated through numerical examples. Fast convergence was observed since six iterations at most were needed to reach convergence, thanks to the proper choice of initial guesses and convergence control parameters.

The current study is limited to fixed concentrated and uniformly distributed harmonic loads and constant moving loads applied to simply supported undamped double-beam systems. Therefore, there is room left to extend the algorithm to other load types and systems with various boundary conditions. Nonetheless, the developed method is a powerful tool that can serve as a reliable benchmark for future investigations.

ACKNOWLEDGMENTS

The financial support from the National Natural Science Foundation of China (Grant Nos. 52122110, 52101322, 52088102, 52001208, and 42076210) and the Oceanic Interdisciplinary Program of Shanghai Jiao Tong University (Grant Nos. SL2021PT302 and SL2020PT201) is gratefully acknowledged.

AUTHOR DECLARATIONS

Conflict of Interest

The authors have no conflicts to disclose.

Author Contributions

Kabutakapua Kakanda: Conceptualization (lead); Data curation (lead); Formal analysis (lead); Methodology (lead); Validation (lead); Writing – original draft (lead); Writing – review & editing (lead). **Hongbo Zhu:** Data curation (equal); Methodology (equal);

Supervision (equal). **Musumari Herman:** Methodology (equal); Writing – original draft (equal); Writing – review & editing (equal). **Panick Kalambay:** Methodology (equal); Writing – original draft (equal); Writing – review & editing (equal). **Zhaolong Han:** Data curation (equal); Funding acquisition (lead); Methodology (equal); Supervision (equal). **Yan Bao:** Methodology (equal); Supervision (equal); Writing – review & editing (equal). **Mengmeng Zhang:** Writing – review & editing (equal). **Dai Zhou:** Supervision (equal); Writing – review & editing (equal).

DATA AVAILABILITY

The data that support the findings of this study are available from the corresponding author upon reasonable request.

REFERENCES

- J. Wang, Z. Zhang, and H. Hua, "Coupled flexural–longitudinal vibrations of Timoshenko double-beam systems induced by mass eccentricities," *Int. J. Appl. Mech. Eng.* **08**, 1650067 (2016).
- H. Deng, K. Chen, W. Cheng, and S. Zhao, "Vibration and buckling analysis of double-functionally graded Timoshenko beam system on Winkler–Pasternak elastic foundation," *Compos. Struct.* **160**, 152–168 (2017).
- X. Zhao, B. Chen, Y. H. Li, W. D. Zhu, F. J. Nkiegaing, and Y. B. Shao, "Forced vibration analysis of Timoshenko double-beam system under compressive axial load by means of green's functions," *J. Sound Vib.* **464**, 115001 (2020).
- S. Hadian Jazi, "Nonlinear vibration of an elastically connected double Timoshenko nanobeam system carrying a moving particle based on modified couple stress theory," *Arch. Appl. Mech.* **90**, 2739–2754 (2020).
- S. Liu and B. Yang, "A closed-form analytical solution method for vibration analysis of elastically connected double-beam systems," *Compos. Struct.* **212**, 598–608 (2019).
- A. Mirzabeigy, R. Madoliat, and C. Surace, "Explicit formula to estimate natural frequencies of a double-beam system with crack," *J. Braz. Soc. Mech. Sci. Eng.* **41**, 223 (2019).
- L. Zhang, Q. Ou, and S. Zhou, "Analytical study of the dynamic response of a double-beam model for a geosynthetic-reinforced embankment under traffic loads," *Comput. Geotech.* **118**, 103330 (2020).
- R. Chawla and V. Pakrashi, "Dynamic responses of a damaged double Euler–Bernoulli beam traversed by a 'phantom' vehicle," *Struct. Control Health Monit.* **29**, e2933 (2022).
- N. Mohammadi and M. Nasirshoabi, "Forced transverse vibration analysis of a Rayleigh double-beam system with a Pasternak middle layer subjected to compressive axial load," *J. Vibroeng.* **17**, 4545–4559 (2015).
- B. Milenković, D. Karličić, and Đ. Jovanović, "Determination of natural frequency and amplitude ratio of a Rayleigh double beam system with a Keer middle layer subjected to compressive axial load," in XI International Conference Industrial Engineering and Environmental Protection (Technical Faculty "Mihajlo Pupin"; University of Novi Sad, Zrenjanin, 2021).
- F. Han, D. Dan, and W. Cheng, "Exact dynamic characteristic analysis of a double-beam system interconnected by a viscoelastic layer," *Compos., Part B* **163**, 272–281 (2019).
- H. Fei, D. Danhui, C. Wei, and Z. Jubao, "A novel analysis method for damping characteristic of a type of double-beam systems with viscoelastic layer," *Appl. Math. Modell.* **80**, 911–928 (2020).
- B. Chen, B. Lin, X. Zhao, W. Zhu, Y. Yang, and Y. Li, "Closed-form solutions for forced vibrations of a cracked double-beam system interconnected by a viscoelastic layer resting on Winkler–Pasternak elastic foundation," *Thin-Walled Struct.* **163**, 107688 (2021).
- W. K. F. Brito, C. D. C. D. Maia, and A. V. Mendonca, "Bending analysis of elastically connected Euler–Bernoulli double-beam system using the direct boundary element method," *Appl. Math. Modell.* **74**, 387–408 (2019).

- ¹⁵J. M. Seelig and W. H. Hoppmann, "Normal mode vibrations of systems of elastically connected parallel bars," *J. Acoust. Soc. Am.* **36**, 93–99 (1964).
- ¹⁶T. R. Hamada, H. Nakayama, and K. Hayashi, "Free and forced vibrations of elastically connected double-beam systems," *Bull. JSME* **26**, 1936–1942 (1983).
- ¹⁷Z. Oniszczuk, "Forced transverse vibrations of an elastically connected complex simply supported double-beam system," *J. Sound Vib.* **264**, 273–286 (2003).
- ¹⁸Z. Oniszczuk, "Free transverse vibrations of elastically connected simply supported double-beam complex system," *J. Sound Vib.* **232**, 387–403 (2000).
- ¹⁹Y. Q. Zhang, Y. Lu, and G. W. Ma, "Effect of compressive axial load on forced transverse vibrations of a double-beam system," *Int. J. Mech. Sci.* **50**, 299–305 (2008).
- ²⁰A. Palmeri and S. Adhikari, "A Galerkin-type state-space approach for transverse vibrations of slender double-beam systems with viscoelastic inner layer," *J. Sound Vib.* **330**, 6372–6386 (2011).
- ²¹P. Koziol, "Wavelet approximation of Adomian's decomposition applied to the nonlinear problem of a double-beam response subject to a series of moving loads," *J. Theor. Appl. Mech.* **52**, 687–697 (2014).
- ²²A. Mirzabeigy and R. Madoliat, "A note on free vibration of a double-beam system with nonlinear elastic inner layer," *J. Appl. Comput. Mech.* **5**, 174–180 (2019).
- ²³M. S. Rahman and Y.-Y. Lee, "New modified multi-level residue harmonic balance method for solving nonlinearly vibrating double-beam problem," *J. Sound Vib.* **406**, 295–327 (2017).
- ²⁴S. Liao, "The proposed homotopy analysis technique for the solution of nonlinear problems," Ph.D. thesis, Shanghai Jiao Tong University, 1992.
- ²⁵S. Liao, *Homotopy Analysis Method in Nonlinear Differential Equations* (Springer, 2012).
- ²⁶A. Sami Bataineh, M. S. M. Noorani, and I. Hashim, "Approximate analytical solutions of systems of PDEs by homotopy analysis method," *Comput. Math. Appl.* **55**, 2913–2923 (2008).
- ²⁷Z. Odibat and A. Sami Bataineh, "An adaptation of homotopy analysis method for reliable treatment of strongly nonlinear problems: Construction of homotopy polynomials," *Math. Methods Appl. Sci.* **38**, 991–1000 (2015).
- ²⁸S. Shahlaei-Far, A. Nabarrete, and J. M. Balthazar, "Nonlinear vibrations of cantilever Timoshenko beams: A homotopy analysis," *Lat. Am. J. Solids Struct.* **13**, 1866–1877 (2016).
- ²⁹M. Turkyilmazoglu, "Convergence accelerating in the homotopy analysis method: A new approach," *Adv. Appl. Math. Mech.* **10**, 925–947 (2018).
- ³⁰P. Sattari Shajari and A. Shidfar, "Application of weighted homotopy analysis method to solve an inverse source problem for wave equation," *Inverse Probl. Sci. Eng.* **27**, 61–88 (2019).
- ³¹H. M. Sedighi, K. H. Shirazi, and J. Zare, "An analytic solution of transversal oscillation of quintic non-linear beam with homotopy analysis method," *Int. J. Non-Linear Mech.* **47**, 777–784 (2012).
- ³²M. Maleki, S. A. M. Tonekaboni, and S. Abbasbandy, "A homotopy analysis solution to large deformation of beams under static arbitrary distributed load," *Appl. Math. Modell.* **38**, 355–368 (2014).
- ³³X. Lin, Y. Huang, Y. Zhao, and T. Wang, "Large deformation analysis of a cantilever beam made of axially functionally graded material by homotopy analysis method," *Appl. Math. Mech.* **40**, 1375–1386 (2019).
- ³⁴M. Chen, M. Zou, and L. Zhu, "Frequency-domain response analysis of adjacent multiple floaters with flexible connections," *J. Ship Mech.* **22**, 1164–1180 (2018).
- ³⁵M. Zou, M. Chen, L. Zhu, L. Li, and W. Zhao, "A constant parameter time domain model for dynamic modelling of multi-body system with strong hydrodynamic interactions," *Ocean Eng.* **268**, 113376 (2023).
- ³⁶C. Xie, L. Zhou, S. Ding, R. Liu, and S. Zheng, "Experimental and numerical investigation on self-propulsion performance of polar merchant ship in brash ice channel," *Ocean Eng.* **269**, 113424 (2023).
- ³⁷Y. Wu and Y. Gao, "Dynamic response of a simply supported viscously damped double-beam system under the moving oscillator," *J. Sound Vib.* **384**, 194–209 (2016).